

# SCINTILLATION-INDUCED INTERMITTENCY IN SETI

James M. Cordes<sup>1,2,3</sup>, T. Joseph W. Lazio<sup>1,2</sup>, & Carl Sagan<sup>1,3,4,5</sup>

## ABSTRACT

We use scattering theory, simulations, and empirical constraints on interstellar scintillations to discuss the intermittency of radio signals from extraterrestrial intelligence (ETI). The number of ETI sources in the Galaxy has a direct influence on the expected dynamic range of fluxes in a survey, through inverse square-law effects and, equally importantly, by the number of independent statistical trials made on modulations caused by interstellar scintillations. We demonstrate that scintillations are very likely to allow initial detections of narrowband signals, while making redetections extremely improbable, a result that follows from the skewed, exponential distribution of the modulation. This conclusion holds for relatively distant sources but does not apply to radio SETI toward nearby stars ( $\lesssim 100$  pc).

Recent SETI has found non-repeating, narrowband events that are largely unexplained. We consider three models in order to assess these events and to analyze large surveys in general: (I) Radiometer noise fluctuations; (II) A population of constant Galactic sources which undergo deep fading and amplification due to interstellar scintillation, consistent with ETI transmissions; and (III) Real, transient signals (or hardware errors) of either terrestrial or extraterrestrial origin.

We derive likelihood and Bayesian tests of the models for individual events and globally on entire surveys. Applying them to The Planetary Society/Harvard META data, we find that Models II and III are both highly preferred to Model I, but that Models II and III are about equally likely. In the context of Model II, the likelihood analysis indicates that candidate events above threshold ( $\sim 32\sigma$ ) are *combinations* of large amplitude noise fluctuations

---

<sup>1</sup>Department of Astronomy, Cornell University

<sup>2</sup>National Astronomy & Ionosphere Center, Cornell University

<sup>3</sup>Center for Radiophysics and Space Research, Cornell University

<sup>4</sup>The Planetary Society, Pasadena, CA 91106

<sup>5</sup>Deceased

and scintillation gains, making it highly probable that events seen once will only very rarely be seen again. Ruling out Model II in favor of Model III is difficult — to do so, many more reobservations (e.g., thousands) are needed than were conducted in META (hundreds) *or* the reobservation threshold must be much lower than was used in META. *We cannot, therefore, rule out the possibility that META events are real, intrinsically steady ETI signals.*

Our formalism can be used to analyze any SETI program. We estimate the number of reobservations required to rule out Model II in favor of Model III, taking into account that reobservations made promptly sample the same scintillation gain as in the original detection, while delayed reobservations sample a decorrelated scintillation modulation. The required number is a strong function of the thresholds used in the original survey and in reobservations.

We assess optimal methods for applying statistical tests in future SETI programs that use multiple site and multiple beam observations as well as single site observations. We recommend that results be recorded on many more events than have been made to date. In particular, we suggest that surveys use thresholds that are far below the false-alarm threshold that is usually set to yield a small number of noise-induced “detections” in a massive survey. Instead, large numbers of events should be recorded in order to (1) demonstrate that background noise conforms to the distribution expected for it; and (2) investigate departures from the expected noise distribution as due to interference or to celestial signals. In this way, celestial signals can be investigated at levels much smaller than the false-alarm threshold. The threshold level for archiving candidate intensities and their corresponding sky positions is best defined in terms of the recording and computational technology that is available at a cost commensurate with other survey costs.

## 1. INTRODUCTION

The commonly anticipated signal in radio searches for extraterrestrial intelligence (SETI) is a narrowband, slowly modulated signal of sustained duration. For example, bandwidths less than 1 Hz and signal durations of days and longer are often hypothesized. These signal characteristics are closely related to the traditional requirement in science for *repeatability* of an experimental or observational result as well as to the hope that members of one class of ETI signal—those that are targeted explicitly to us—will sustain themselves long enough to establish repeatability.

By contrast with such an idealized type of signal, it is easy to imagine other kinds of received signals that depart significantly from the idealization, particularly with regard to duration and amplitude stability. Moreover, several recent searches have found signals that are narrowband, do not match the characteristics of known, interfering signals of terrestrial or solar system origin, and yet, do not repeat when follow-up observations of the relevant sky positions are performed. The META project (Horowitz & Sagan 1993; hereafter HS93) found several dozen such signals at 1420 and 2840 MHz. Similarly, SERENDIP III has found  $\gtrsim 100$  transient candidate events at 430 MHz (Bowyer, Werthimer, & Donnelly 1994). An older example of this kind is the “WOW!” signal found in the Ohio State SETI program at 1420 MHz (Dixon 1985). For META the characteristic signal duration is no more than  $\sim 1$  minute and all reobservation attempts—ranging from minutes to years after receipt of the original candidate signal—have failed. Intense scrutiny of the WOW sky position (e.g., Gray 1995) has also failed to redetect a signal.

A feature common to all SETI programs is that, by virtue of the multidimensional search space (direction, frequency, duration, etc.), large numbers of independent statistical tests are performed, typically  $\sim 10^{13}$ – $10^{14}$ . The aim is to separate noise, interference, and candidate real signals. This winnowing process is based on the rigorously known properties of background noise and on an ad hoc expert system designed to reject terrestrial signals which fail sidereal and doppler requirements that bona fide celestial signals must satisfy. As a result of the large number of trials, even pure noise can produce large amplitudes that are statistically highly improbable in a single trial. Similarly, unusual interference, whether of natural or artificial origin, that fails to be identified by rejection algorithms can be recorded as candidate signals.

In this paper, we address signal intermittency in SETI programs. Our goals are to 1) develop the statistical apparatus for interpreting transient signals; 2) assess surveys, particularly META (HS93), that have yielded nonconfirmed events; 3) prescribe optimal methods for reporting the results of ongoing SETI programs; and 4) improve the search protocols of future SETI programs.

A short list of possible explanations for intermittency includes:

1. Noise in the receiver electronics, including thermal noise, cosmic ray induced events, and hardware failures;
2. Radio frequency interference (RFI) whose origin is terrestrial, from Earth orbit, or from interplanetary spacecraft;
3. Natural, extrinsic modulation of narrowband astrophysical sources such as that caused by interstellar (radio) scintillation (ISS) or gravitational lensing;

4. Natural, extrinsic modulation of ETI sources; and
5. Intrinsic intermittency at the source of an ETI signal due to natural causes, such as planetary rotation or the nature of the transmission (e.g., planetary radar) or, for deliberate reasons, to frustrate detection and decryption by non-target civilizations.

Causes (2) and (5) are not dissimilar in their transmission properties though their sidereal and doppler properties may allow them to be distinguished. In this paper, we use a Bayesian likelihood analysis as the apparatus for comparing cause (4) with several of the other, plausible explanations for signal intermittancy.

Our focus on cause (4), with particular emphasis on ISS, is motivated by two considerations. First, it is the simplest possible explanation for the transient behavior of signals that *perhaps* otherwise would be steady. Second, ISS is important at centimeter wavelengths (Rickett 1990) that are commonly used in searches for ETI. Centimetric wavelengths are often favored because background noise levels are minimized relative to other wavelength bands and it is argued that spectral lines from HI and OH in this “waterhole” band serve as signpost or “magic” frequencies at which to transmit and receive (Oliver 1973). Most importantly, however, we find that ISS *by itself* is sufficient to explain the lack of confirmation of any ETI candidate signals in surveys conducted to date.

We consider ISS at waterhole frequencies using the framework of Cordes & Lazio (1991) and a recent model for Galactic free electrons by Taylor & Cordes (1993). We show that the properties of scintillations expected from a Galactic population of ETI sources are intimately related to the *number* of such sources, if quasi-uniformly distributed, thought to exist in the Galaxy. This follows because the time scale and characteristic bandwidth are strongly dependent on the distance of the source. In addition, the maximum increase in amplitude due to scintillation expected for any source is related to the number of statistical trials made and is therefore also related to the number of sources in the Galaxy.

In previous papers (Cordes & Lazio 1991; Cordes & Lazio 1993; Lazio & Cordes 1998, hereafter CL91, CL93, & LC98, respectively), we have emphasized the need for multiple observations of the sky in order to combat the effects of interstellar scintillations. In particular, we have found that the optimal number of observations of a specific direction is a few and that these can restore some of the detection probability that would be lost otherwise in a single pass on the sky. Here, we focus on reobservations of an initial candidate detection and find a seemingly contradictory result: namely, that to rule out the reality of the candidate signal, it takes hundreds, if not thousands, of reobservations to do so.

In §2 we summarize the effects scintillations impose on celestial signals from compact sources. In §3 we discuss the distribution of a Galactic population of extraterrestrial

civilizations and, for simplicity, we assume that the Galactic population is a set of “standard candle” transmitters. In §4 we summarize some recent SETI programs and the candidates they detected. Basic issues underlying an interpretation of survey results are outlined qualitatively in §5 while in §6 we introduce the likelihood functions that form the basis of our quantitative analysis. In §7 we analyze individual candidate events assuming that any multiple observations occur at times such that interstellar scintillations are uncorrelated; correlated scintillations are treated in §8. In §9 we extend our likelihood analysis to surveys as a whole.

We extend our analysis to two-station SETI in §10 where we show that many of the challenges in verifying scintillating signals at a single site persist for simultaneous observations made at a pair of sites. We propose an alternative detection scheme in §11 that uses all of the data in a survey and is much more sensitive than a signal-to-noise ratio limited survey. Our analyses are distilled into recommendations for future SETI in §12 and in §13 we present our conclusions.

In Appendix A we define symbols used throughout our analysis and Appendix B discusses scintillating source properties, including detection probabilities at single and multiple sites.

## 2. INTERSTELLAR SCINTILLATIONS (ISS)

In CL91, CL93, & LC98, we have described the impact upon source detection procedures resulting from radio waves propagating through a random, phase-changing medium, such as the ionized interstellar medium (ISM) or the interplanetary medium (IPM). The reader is directed to those papers for details on the salient features of scintillations (also see Rickett 1990). Here we summarize scintillation phenomena that are relevant to our analysis.

### 2.1. Brief Summary

The scattering regime in which we are most interested is that which produces saturated intensity scintillations. In this *strong scattering* case, intensity variations branch into two forms (Rickett 1990): fast, diffractive scintillations (DISS) and slow, refractive scintillations (RISS). DISS is manifested as 100% variations of the intensity in both time and frequency. The characteristic time and frequency scales are discussed below. RISS typically shows 10–20% variation on times scales of days to months and is correlated over a wide range of

frequency. At centimeter wavelengths, most of the Galaxy is seen in the strong scattering regime. For sources near the Sun, e.g.,  $< 100$  pc at 1 GHz, weak scintillations occur. A transition region extending to about 500 pc at 1 GHz produces scintillations with greater than 100% intensity variations (c.f. LC98; Rickett 1990). Consequently, in the remainder of this paper, we shall concentrate on the impact of strong scattering on SETI surveys done to date. Also, we discuss only the effects of DISS because modulations from it are orders of magnitude larger than those from RISS in large-scale SETI.

While our interest here is primarily on *intensity variations* from interstellar scattering, phase fluctuations induced by the medium may also manifest themselves as *Doppler shifts* or *frequency wandering* of narrow spectral lines (CL91). In SETI programs optimized for finding narrowband signals, follow-up observations on candidate signals need to account for the possibility that signals drift or shift in frequency on a variety of time scales. Drifts may be caused by interstellar scattering, interplanetary scattering in the solar wind, and, presumably, in the stellar wind of the transmitting civilization’s host star. These drifts are much less than the Doppler shifts caused by the spin or orbital motion of a planet. Nonetheless, they must be taken into account when making follow-up observations of candidate signals because they can still span several to many frequency bins of a narrow-band spectrometer.

## 2.2. Characteristic Time and Frequency Scales

The intensity of a scintillating source is correlated on characteristic time and frequency scales: the scintillation time,  $\Delta t_d$ , and the scintillation bandwidth,  $\Delta \nu_d$ . For the vast majority of lines of sight, the scintillation bandwidth exceeds the anticipated intrinsic widths of deliberately transmitted lines ( $\lesssim 1$  Hz). In addition, broadening of the line by propagation effects is much less than 1 Hz for most lines of sight. Therefore, assuming intrinsic line widths are not substantially less than 1 Hz, the line shape is essentially unaffected by scattering while the line amplitude is modulated for most lines of sight (Drake & Helou 1977; CL91).

When scintillations are saturated and the line shape undergoes negligible changes, the only astrophysically variable parameter is the scintillation time scale,  $\Delta t_d \propto \nu^{1.2}/V_\perp$  where  $V_\perp$  is a characteristic transverse speed that is a combination of the velocities of the source, observer, and medium. The time scale also depends on distance, with more distant sources having shorter time scale scintillations. For a medium with homogeneous statistics,  $\Delta t_d \propto D^{-0.6}$  (Cordes & Lazio 1991), but the dependence is more complex for a realistic model of the Galaxy, as discussed below. The time scale has been measured to be seconds

to hours for pulsars (Cordes 1986), whose transverse velocities dominate the relevant  $V_{\perp}$  and are in the range of 30 to 2000 km s<sup>-1</sup> (Harrison & Lyne 1993; Cordes, Romani & Lundgren 1993; Lyne & Lorimer 1994). By comparison, the motions of main sequence stars in the Galaxy and the orbital motions of their planetary companions are much lower than the average pulsar speed. Therefore, we expect that an ETI source at the same distance as a given pulsar will show a characteristic scintillation time scale that is much longer than that seen from the pulsar, by typically an order of magnitude. We point out that differential galactic rotation does not play a large role because the scattering material also participates in the rotation (Cordes 1986). We also emphasize that, as the scintillation time is frequency dependent, an assessment of the role of scintillations must take the observation frequency into account.

Through modeling of the free electron density in the Galaxy, it is possible to estimate the scintillation time scale for ETI sources. The most recent model for the free electron density and its fluctuations (Taylor & Cordes 1993) incorporates all available data on pulsar distances and dispersion measures, and radio scattering data on pulsars, Galactic maser sources, and extragalactic sources viewed through the ISM.

Figure 1 shows contours of the scintillation time  $\Delta t_d$  for directions in the plane of the Galaxy (i.e., Galactic latitude  $b = 0$ ). We have assumed a transverse speed  $V_{\perp} = 10$  km s<sup>-1</sup> for all ETI sources and an observation frequency of 1.42 GHz. Given the range of possible orbital motions and motions in the Galaxy, the effective velocity could vary by a factor of two or more, either lower or higher. It is evident that the scintillation time scale is of order minutes only for the most distant regions of the Galaxy. For most directions, it is typically hours.

The scintillation time scale, therefore, significantly exceeds the typical time spent on a given sky position in SETI unless all sources are in the Galactic plane at large distances. Consequently, one may consider any putative (intrinsically steady) ETI signal to be constant over the observation time, though scintillations may have modulated it significantly upward or downward in apparent strength relative to its long term mean. Prompt repeat observations of a candidate signal made sooner than one diffraction time scale after an initial, tentative detection will “see” the same signal strength. Conversely, repeated observations made at times when the scintillation modulations are mutually independent will detect a large range of signal strengths that follows the distribution of scintillation modulations. For saturated scintillations, this distribution is a one-sided exponential function.

The reader may think that Fig. 1 can be used to dismiss immediately candidate signals in META as being due to RFI, since they are not redetected immediately after their initial

detections. This is not the case. As we show below, candidate signals can be detected in META-like surveys as a *combination* of noise fluctuations and scintillations of celestial signals. The noise decorrelates immediately, so even a persistent source can disappear into the noise after an initial detection.

Figure 1 also shows the scintillation bandwidth,  $\Delta\nu_d$ , at 1.42 GHz. The scintillation bandwidth is found to be much greater than the hypothesized signal bandwidth ( $\lesssim 1$  Hz) of deliberate ETI signals for all lines of sight through the Galaxy. The diffraction bandwidth scales with frequency as  $\Delta\nu_d \propto \nu^{4.4}$ .

The reciprocals of the scintillation time scale and bandwidth are also of potential interest, yielding the bandwidth of *spectral broadening* and the *pulse-broadening* time, respectively, as  $\Delta\nu_{sb} = (2\pi\Delta t_d)^{-1}$  and  $\tau_d = (2\pi\Delta\nu_d)^{-1}$  (e.g., Lovelace 1970; CL91, CL93). Using values for the scintillation time scale  $\Delta t_d$  from Fig. 1, it is clear that spectral broadening  $\ll 1$  Hz at 1.42 GHz. This confirms our previous statement that line shapes are essentially unaltered by scattering if they are intrinsically wider than the spectral broadening from scattering.

### 2.3. Detection Probabilities

Intensity statistics are discussed in Appendix B. There we distinguish variations of the intensity over short time scales, when the scintillation modulation is constant, from those over long times when the modulation varies according to its exponential distribution (in strong scattering). In the former case the intensity probability density function (pdf) is that for a phasor of constant amplitude  $gS$  combined with noise, where  $g$  is the scintillation “gain” and  $S$  is the source intensity in the absence of scintillations. The pdf  $f_I(I; gS)$  is given in Eq. B4, with  $S \rightarrow gS$ . In the second case, where  $g$  varies over its sample space, the pdf,  $f_{I,\text{scint}}(I; S)$ , is a simple, one-sided exponential with mean  $\langle I \rangle = S + \langle N \rangle$ , where  $S$  is assumed to be constant and  $N$  is radiometer noise.

Each pdf implies a *detection probability* that the intensity exceeds a specified threshold intensity,  $I_T$ . We call these  $P_d(I_T; S)$  and  $P_{d,\text{scint}}(I_T; S)$ , respectively, and define them in Eq. (B8)–(B9). When there is no signal, just noise,  $S = 0$ , the detection probability is the false-alarm probability. In Fig. 2 we show detection probabilities with and without scintillations for the case where the false-alarm probability is  $10^{-12}$ , corresponding to a threshold  $I_T \langle N \rangle = \log 10^{+12} = 27.6$ . Recent SETI programs do, in fact, achieve conformance to exponential statistics up to large thresholds such as this so long as terrestrial RFI is removed (cf. Figure 4 of HS93; Levin *et al.* 1995).



We reiterate a point discussed at length in our earlier papers: In the absence of scintillations, a source is essentially undetectable if  $S < I_T$ , i.e.,  $P(I > I_T) \approx 0$ . However, by the multiplicative nature of the scintillation gain, otherwise undetectable sources can be modulated above threshold. Since  $g$  is drawn from an exponential distribution, it can reach large values that result in a detection probability,  $P_d(I_T, gS)$ , significantly in excess of its value in the absence of scintillations,  $P_d(I_T, S)$ . Modulations which increase the signal strength are not the norm, though, and are in fact less likely than the converse. In contrast to our earlier papers (CL91, CL93, LC98), where we considered the probability of detecting a source at least once, in a survey, say, here we consider the probability of detecting a source at least twice, once in a survey and then again in a set of reobservations.

## 2.4. Second-order Statistics

Appendix B also presents results on second-order statistics that we use in discussing correlations in scintillation gain between several observations of the same source. Of particular interest is the conditional probability that a signal is detected in a second observation given that the intensity had the value  $I_1$  in an initial “detection,”  $P_{2d}(I_T|I_1; S, \rho_g[\Delta t])$ . Here  $\Delta t$  is the time interval between observations and  $\rho_g$  is the autocorrelation function of the scintillation gain, normalized to  $\rho_g(0) \equiv 1$ . This function is gaussian-like in form and has a width equal to the characteristic (diffractive) scintillation time,  $\Delta t_d$ .

In Fig. 3 we show the conditional probability plotted against the correlation coefficient  $\rho_g \in [0, 1]$  for several values of the normalized source strength  $\zeta \equiv S/\langle N \rangle$ , threshold  $\eta_T \equiv I_T/\langle N \rangle$ , and intensity  $\eta_1 \equiv I_1/\langle N \rangle$  for an initial detection. As we discuss in §10, observations made at two different sites may also be analyzed using Fig. 3. Like two temporally-spaced observations, the scintillation gain is partially correlated according to a spatial correlation function,  $\rho_s$ .

Figure 3 illustrates the importance of the combined effects of noise and scintillation. For values typical of META,  $\eta_1 = 32$  and  $\eta_T = 20$ , the probability  $P_{2d}$  is less than unity for a nominally detectable signal,  $\zeta = 32$ , even for perfectly correlated scintillation gains. If we suppose that the initial detection,  $\eta_1$ , occurred because of the scintillation amplification of a weaker signal, e.g.,  $\zeta \leq 16$ , the chances of *not* detecting the signal during reobservations are even greater. Combinations of  $\zeta$  and  $\rho$  can produce  $P_{2d} \ll 0.1$  in some cases.

We will demonstrate that, in large scale surveys involving large numbers of statistical trials, threshold crossings (initial “detections”) will occur through the combined effects

of noise and scintillating phasors (in the case where ETI signals exist!). Because of this “scintillation-noise conspiracy,” *confirmations* of detected signals are difficult, owing to the rapid decorrelation of the noise on short time scales. Thus, for large surveys with large detection thresholds, the probability of redetection is small and, therefore, the absence of confirming redetections is insufficient evidence for concluding the absence of a possibly steady ETI signal. Similarly, *simultaneous* observations at two sites, where radiometer noise is uncorrelated, allow detection at one site and nondetection at the other with large probability.

Qualitatively, noise by itself—without aid from scintillation— can also assist survey detection while inhibiting redetection. But quantitatively, for thresholds, candidate numbers, and numbers of reobservation trials like those in META, it is difficult to explain noise-assisted survey detections combined with the failure of all reobservations. Evidently, scintillations are needed to explain both. The reason lies in the difference in shapes of the detection probability curves in Figure 2 for intensity ratios  $S/I_T \lesssim 1$ . These, in turn, arise because, even though noise and scintillations both have one-sided exponential pdf’s, they act asymmetrically because scintillations act multiplicatively on the true signal, while noise is additive.

## 2.5. Scintillations as a Reality Check on Candidate Sources

If a candidate signal is also detected in the reobservation phase of a SETI program, scintillations can serve to confirm that the candidate signal is in fact coming from beyond the solar system (cf. HS93). The strength of a signal from a candidate source should vary from observation to observation in a manner consistent with the exponential distribution, provided the observations are separated by more than a scintillation time and, of course, that scintillations are strong.

In CL91, we alluded to another scintillation phenomenon, *spectral wandering*. If observed over time periods shorter than the scintillation time, the centroid of a narrow-band signal will show random but correlated shifts in frequency in addition to any Doppler shifts. If the signal is averaged over times much larger than the scintillation time, the signal will be spectrally broadened, i.e., the spectral shape of the signal will converge to a Gaussian-like shape with width  $\Delta\nu_{sb} \sim 1/\Delta t_d$  (CL91).

Expressions are presented in CL91 for  $\Delta\nu_{sb}$  as a function of distance and frequency for both weak and strong scintillation regimes. For Galactic sources, we expect frequency wandering to be roughly the reciprocal of the scintillation time scale. Reference to Fig. 1

shows that wandering will be at the level of  $10^{-4}$  to 0.1 Hz. There are some directions for which the level of scattering is underestimated by the model used to construct Fig. 1. For these directions (such as sources in or beyond the Galactic center), the spectral wandering can exceed 0.1 Hz.

### 3. GALACTIC ETI TRANSMITTERS

In this section, we show that the number of ETI transmitters in the Galaxy influences the expected distribution of source fluxes and determines the scintillation properties of the sources as manifested in a particular survey.

#### 3.1. Demography

Suppose the number of transmitting civilizations in the Galaxy is  $N_D$  as estimated, for instance, from the Drake equation (Shklovskii & Sagan 1966). The number density of sources is

$$n_D = \frac{N_D}{2\pi R_G^2 H_G}, \quad (1)$$

assuming that all civilizations reside in a disk of radius  $R_G$  and thickness  $2H_G$ .

The volume through the Galactic disk sampled by a radio telescope of beam solid angle  $\Omega_b$  is  $V_b = \Omega_b D^3/3$ , where  $D$  is the characteristic distance through the disk,  $D \approx \min(H_G/\sin|b|, R_G)$ , where  $b$  is the Galactic latitude.  $D$  is direction-dependent, but observations in the plane will yield  $D \sim R_G$ . The number of sources in a typical beam is

$$N_b = n_D V_b \sim 10^{-2.7} N_D \left(\frac{D}{R_G}\right)^3 \left(\frac{R_G/H_G}{150}\right) \left(\frac{\theta_b}{1 \text{ deg}}\right)^2, \quad (2)$$

where  $\theta_b$  is the one-dimensional beam width (FWHM) and we assume  $R_G/H_G = 150$ . If there are more than about  $10^3$  sources in the Galaxy, every telescope beam (of 1 deg size) will contain at least one source, on average. It is convenient to rewrite  $N_b$  as

$$N_b = \left(\frac{D}{D_{\text{mfp}}}\right)^3 \quad (3)$$

where the ‘‘mean free path’’ for encountering a source in the beam is

$$D_{\text{mfp}} = \left(\frac{3}{n_D \Omega_b}\right)^{1/3} \approx R_G \left(\frac{501}{N_D}\right)^{1/3} \left(\frac{150}{R_G/H_G}\right)^{1/3} \left(\frac{1 \text{ deg}}{\theta_b}\right)^{2/3} \quad (4)$$

The typical distance between sources is

$$\ell_D \sim \begin{cases} H_G \left(\frac{2}{3}\right)^{1/2} \left(\frac{\tilde{N}_D}{N_D}\right)^{1/2} \left[1 + \frac{N_D}{2\tilde{N}_D}\right]^{1/2} & N_D \leq \tilde{N}_D; \\ H_G \left(\frac{\tilde{N}_D}{N_D}\right)^{1/3} & N_D \geq \tilde{N}_D, \end{cases} \quad (5)$$

where  $\tilde{N}_D$  is the number of sources such that  $\ell_D$  equals one scale height of the Galactic disk ( $H_G$ ):

$$\tilde{N}_D = \frac{3}{2} \left(\frac{R_G}{H_G}\right)^2 = 10^{4.5} \left(\frac{R_G/H}{150}\right)^2. \quad (6)$$

Analogous expressions can be derived for a spherical distribution of ET sources. The concentration of META candidates toward the Galactic plane motivates our focus on a disk population, however.

Finally, although we assume the strong scattering regime throughout this paper, there may be sources within the weak or transition scattering regimes if the number of civilizations in the Galaxy exceeds  $10^5$  and  $10^3$ , respectively. These numbers follow from our estimates in §2.1 for the distances to which weak or transition level ISS occurs and matching these to Eq. 5 and solving for  $N_D$ . Also, the population of Galactic ET civilizations can be as large as  $10^5$  depending on what fraction of the unaccounted-for events in META are, in fact, due to ETI sources (HS93).

### 3.2. Source Strengths of Standard Candle Transmitters

A Galactic population of transmitters, each radiating with effective isotropic radiation power (EIRP)  $\mathcal{P}$ , will show maximum and minimum fluxes,

$$S_1 = \mathcal{P}/4\pi\ell_{\min}^2 \quad (7)$$

$$S_0 = \mathcal{P}/4\pi\ell_{\max}^2 \quad (8)$$

from the nearest and furthest sources, respectively.<sup>1</sup> Within these bounds, the pdf for  $S$  is

$$f_S(S) = \left(\frac{\alpha - 1}{S_0}\right) \left[1 - (S_0/S_1)^{\alpha-1}\right]^{-1} \left(\frac{S}{S_0}\right)^{-\alpha}. \quad (9)$$

---

<sup>1</sup> For simplicity, we ignore transmitter beaming in our analysis. Beaming away from us clearly extends the minimum flux  $S_0$  to zero. The net effect, of course, is to decrease the probability of detecting strong sources when there is a fixed number of transmitters in the Galaxy.

Disk and spherical populations are described by  $\alpha = 2$  and  $\alpha = 5/2$ , respectively, as is well known in studies of natural radio sources (Scheuer 1974; Condon 1974) and  $\gamma$ -ray sources (Wasserman 1992).

Taking  $\ell_{\min} \sim \ell_{\text{D}}$ , and  $\ell_{\max} \sim R_{\text{G}}$ , we find that  $S_1/S_0 \sim N_{\text{D}}$  for  $N_{\text{D}} \leq \tilde{N}_{\text{D}} \sim 10^{4.5}$ . In the large civilization limit ( $N_{\text{D}} \gtrsim \tilde{N}_{\text{D}}$ ), the scaling is  $S_1/S_0 \sim (R_{\text{G}}/H_{\text{G}})^2 (N_{\text{D}}/\tilde{N}_{\text{D}})^{2/3} \sim 10^{4.4} (N_{\text{D}}/\tilde{N}_{\text{D}})^{2/3}$  (c.f. Eq. 5). Depending on the abundance of transmitting civilizations in the Galaxy, the dynamic range of source fluxes may be modest or extremely large.

In reality, radio transmission powers from Galactic civilizations will be described by a luminosity function for  $\mathcal{P}$  that incorporates technological and sociological evolution. Since we do not know the form of the luminosity function, we will make use of the “standard candle” form of Eq. 9 in the remainder of the paper, keeping in mind that it is essentially a place holder for what may be a quite different distribution of source strengths.

## 4. SURVEY PROGRAMS

In this section we summarize current and recent survey programs; see also Table 1.

### 4.1. The META Program

Horowitz & Sagan (1993) summarize the META Survey that uses a  $2^{23}$  point Fourier transform spectrometer to analyze a total bandwidth of 400 kHz (0.05 Hz resolution). Two observing frequencies were analyzed: 1420 MHz in the “waterhole,” and its harmonic at 2840 MHz. Spectra were obtained in 20 s data spans at each sky position after adjusting for the Doppler shift from the Earth’s motion relative to each of three reference frames: the local standard of rest, the Galactic barycenter, and the cosmic microwave background. Over a five-year period, about  $6 \times 10^{13}$  combinations of spectral channels and sky positions were investigated. Most of these, of course, yielded amplitudes consistent with the expected exponential noise. After removing obvious, terrestrial interference and setting a threshold such that few, noise-only events would exceed it, 74 events remained. Of these, half could be rejected through further investigation as being due to terrestrial interference, cosmic ray events in the semiconductors of the spectrometer, and other processor errors.

The remaining 37 candidates include 14 at 1420 MHz and 23 at 2840 MHz with approximately equal numbers of candidates in each of the three reference frames. Of these 37 events, 26 are formally below the false-alarm threshold ( $\sigma \ln 6 \times 10^{13} = 31.7\sigma$ ) defined

so that one event should exceed the threshold in the entire survey. HS93 comment that the 26 events below  $31.7\sigma$  are consistent with the exponential distribution expected from pure noise. Consequently, in our analysis, we restrict our attention to the 11 events in Table 2 of HS93 with amplitudes  $> 31.7\sigma$  and especially to those 9 events larger than  $33\sigma$ .

When a candidate detection occurred, the real-time data acquisition system made reobservations of the sky position in the relevant reference frame beginning about 40 s after the initial detection and ending about 3 min afterward, when the source had drifted out of the primary beam of the telescope (when used as a transit instrument). It is notable that *none of the candidate positions showed evidence for a signal in any of the reobservations, either within minutes after the initial detection, or days, months, or years later.* The effective detection threshold in reobservations was significantly lower than in the main survey observations, being typically 20 times the mean noise level.

If all 37 META events that survive culling are due to ETI, there must be  $> 10^5$  transmitting sites at 1420 and 2840 MHz in the Galaxy (HS93), based on a simple scaling of META’s “duty cycle” in scanning the sky.

## 4.2. The META II Program

The META II system uses back-end hardware identical to that of META on a 30 m antenna in Argentina (Colomb et al. 1993). The observation frequency is 1.42 GHz. Like META, META II finds extrastatistical events that are not redetected when observations are made at the appropriate sky positions. Reobservations are made both promptly and with substantial delay of a day or more. For about 25% of the time since 1993 November, observations have been made simultaneously with META and META II in the overlapping sky region of  $-30 \text{ deg} \leq \delta \leq -10 \text{ deg}$ .

## 4.3. The SERENDIP III Program

The SERENDIP III program (Bowyer et al. 1994) has been operated at the Arecibo Observatory since 1992 April in a “piggyback” mode whereby pointing of the antenna is under control of other investigators, thus yielding semi-random but complete coverage of the Arecibo sky. In this program, a 12 MHz bandpass centered at 0.43 GHz is analyzed in 2.5 MHz wide subbands. An FFT spectrometer obtains 4M point spectra in 1.7 s at each of 5 subbands for a channel width of 0.6 Hz. The program has covered 89% of the observable sky at Arecibo (28% of the entire sky) at least once and about 18% of the observable sky

has been observed at least 5 times. The threshold is  $15\sigma$  and no explicit reobservations are made. During the survey, a total of  $4 \times 10^{13}$  channel-sky position observations have been made in 4500 hr of observations.

## 5. BASIC ISSUES IN ANALYZING SURVEY EVENTS

In the following we compare alternative explanations for the candidate events in a survey. For definiteness, we cast the discussion in terms of the META survey, though our formalism is general. We stress the fact that, in META, no signals were detected in any reobservations of the relevant sky positions.

### 5.1. Models for Survey Events

The models we consider are:

**Model I:** The measured signal consists only of radiometer noise in both the survey and the reobservations.

**Model II:** The measured signal results from noise combined with a real celestial signal of average strength  $S$  that has scintillated into an improbably strong amplitude, with gain  $g$  in the survey, but has remained below threshold in the reobservations. We assume that the signal would be constant were it not modulated by scintillations.

**Model III:** The survey detection results from a real, *transient* signal of either celestial or terrestrial origin that does not repeat in any of the reobservations.<sup>2</sup> Terrestrial origins for the survey detection would include radio frequency interference (RFI) or cosmic ray events and failures in the electronics. We characterize the transient signal in the survey as an amplitude  $S_{\text{RFI}}$ .

In Fig. 4 we show simulated time series for the three models.

Models II and III are similar in that the survey is assumed to have acquired events that are extremely rare, whether due to atypical forms of RFI that pass through RFI-rejection

---

<sup>2</sup> One may compare the SETI case with gamma-ray bursts (GRB), which do not repeat, but have been identified as extraterrestrial sources. This identification relies on the fact that terrestrially produced GRBs that would interfere with the detection of astronomical bursts are rare, thankfully, and because many GRBs have been observed with more than one spacecraft, allowing time-of-arrival constraints on their directions.

filters or to rare scintillation peaks of real celestial sources. Surveys that sift through tens of teraevents are indeed likely to yield such rare occurrences.

In later sections we shall compare, in a quantitative sense, the viability of these three models in interpreting candidate events and their evident nonrepeatability. While it is tempting to dismiss the events as a rare kind of RFI, we take the point of view that one should be able to show quantitatively that Model III is superior to Model II. We also anticipate that future surveys will yield similar events that will demand assessment and that some may eventually show successful detections in the reobservations. Therefore, we shall also explore optimal methods for conducting and reporting future SETI programs.

## 5.2. General Considerations on Scintillation Amplitudes

Some simple facts about scintillations and the demography of transmitting sites in the Galaxy suggest that Model II may not be dismissed so easily. In the large number of trials conducted in META ( $6 \times 10^{13}$ ), it is remarkable that *only* 37 remaining signals are unidentified and, for the most part, they satisfy some of the requirements expected for a real ETI signal: a narrowband spectral line in a rest frame of celestial interest. If we interpret the nonrepeatability of the candidates to be the result of scintillation modulation, rather than to intrinsic variability, then it must be assumed that the scintillation gain was extraordinarily high at the time of the detection but was at more probable levels in all reobservations. In order for this to be a likely scenario, the number of statistical trials must be large enough so as to make it probable that a large scintillation gain occurred 37 times during the META survey. The probability of large gains, in turn, is closely related to the number of signals transmitted from all ETI sites in the Galaxy.

As before, let  $N_D$  be the number of ETI civilizations in the Galaxy, each transmitting  $N_{\text{lines}} \geq 1$  spectral lines. These lines may or may not be in bands observed by META or in any other survey. A small multiplicity of lines is advantageous for combatting interstellar scintillation (Cohen & Charlton 1995; Cordes & Sullivan 1995). If no “magic” frequencies or reference frames are believed to pertain to the choice of frequency, the best we can do *a priori* is specify a (large) spectral domain of bandwidth  $B_D$  for the possible frequencies of transmission. The total number of “scintillation trials” for a full sky survey is

$$N_{\text{trials,ISS}} \sim N_D N_{\text{lines}} K_s P_\nu, \quad (10)$$

for  $K_s$  trials per sky position and where  $P_\nu$  is the probability that the observed frequency band in a survey does, in fact, contain signals from ETI sources when a telescope is pointed toward a given source. In the optimistic case, where the choice of frequency bands is



believed to be the proper one and that one or more of the transmitted lines for each and every civilization falls into one of the chosen bands,

$$P_\nu = 1. \quad (11)$$

However, if all frequencies in a large spectral domain  $B_D \gg \Delta\nu_{\text{spectrometer}}$  are equally probable, then

$$P_\nu \approx \frac{N_\nu N_{\text{frames}} \Delta\nu_{\text{spectrometer}}}{B_D} \ll 1. \quad (12)$$

Let  $P_g(g_{\text{max}}) = \exp(-g_{\text{max}})$  be the probability that a scintillation gain  $g_{\text{max}}$ , or larger, occurs. Combined with the number of scintillation trials, we constrain values of  $g_{\text{max}}$  using

$$N_{\text{trials,ISS}} P_g(g_{\text{max}}) \sim N_{\text{cand}} \quad (13)$$

or

$$g_{\text{max}} \sim \ln \left[ \frac{N_D N_{\text{lines}} K_s P_\nu}{N_{\text{cand}}} \right]. \quad (14)$$

Using values for META from the previous section

$$g_{\text{max}} \sim \ln (0.11 N_D N_{\text{lines}} K_s P_\nu). \quad (15)$$

The meaning of Eq. 15 is that if one wants to invoke *likely* values for scintillation gains to account for candidate events, the gains must not strongly exceed a well-defined value, namely  $g_{\text{max}}$ . Given that there must be at least as many transmitters as there are candidates,  $N_D \geq N_{\text{cand}}$ , it may be concluded that  $g_{\text{max}}$  can range from a value of order unity if there are few signals transmitted from sources in the Galaxy (in bands that have been observed) to a value that is easily in the range of 10 to 20 if ETIs abound in the Galaxy ( $N_D \gg 1$ ) or are profligate in their use of the radio spectrum ( $N_{\text{lines}} \gg 1$ ).

If  $g_{\text{max}}$  is large, the intrinsic source strength can be proportionately smaller. For candidate events with intensities  $I_{\text{cand}}/\langle N \rangle \sim 32\text{--}40$ , say, the intrinsic source strength (i.e., in the absence of ISS) need be only  $I_{\text{cand}}/(g_{\text{max}}\langle N \rangle)$ , which could be just a few if  $g_{\text{max}} \sim 10$  to 20. Since the survey threshold in META was  $\sim 32\langle N \rangle$  and the reobservation threshold was  $\sim 20\langle N \rangle$ , the implication is that common values of the scintillation gain will render the signal undetectable, even with a large number of reobservations. For example, in 100 reobservations of a specific source, the maximum likely scintillation gain is  $\ln 100 = 4.6$ , yielding signal amplitudes  $gS \lesssim gI_{\text{cand}}/g_{\text{max}} \lesssim 15\langle N \rangle$ , too small to be detected in reobservations.

### 5.3. General Considerations on Noise Amplitudes

Compared to the number of independent ISS tests, an enormous number of independent trials is made with respect to noise. This number is

$$N_{\text{trials,noise}} \sim N_{\text{ch}} N_{\nu} N_{\text{frames}} N_{\text{pol}} K_{\text{s}} N_{\text{sky}}, \quad (16)$$

where  $N_{\text{sky}}$  is the number of independent sky positions searched. As stated before,  $N_{\text{trials,noise}} \sim 6 \times 10^{13}$  for META. For the simplest spectral analysis of an unsmoothed FFT spectral estimate, the noise in the spectrum is distributed exponentially (c.f. Eq. B4 with  $S = 0$ ) and the false-alarm probability is specified so that  $N_{\text{trials,noise}} P_{\text{fa}} \sim 1$ . For META, the corresponding threshold is about  $32\langle N \rangle$ . This implies that much more modest amplitudes, say  $16\langle N \rangle$ , occur many times ( $\sim \sqrt{N_{\text{trials,noise}}} \sim 10^7$  for META) during the survey. We will find in our analysis below that these modestly frequent noise spikes, combined with rare scintillation gains, play a key role in determining the likelihood function for signals from ETI sources.

## 6. LIKELIHOOD FUNCTIONS OF META-LIKE SURVEYS

To quantify a survey, we define  $N_{\text{sky}}$  as the number of independent sky positions (or telescope beam areas) considered;  $N_{\text{ch}}$  the number of independent frequency channels; and  $K_{\text{s}}$  the number of independent observations or trials made per sky position. Consider a survey that yields  $N_{\text{cand}}$  candidate events having amplitudes  $I^{(\text{su})}(j)$  above a threshold  $I_{\text{T}}^{(\text{su})}$ . The results of the survey may be described as the set of candidate signal intensities

$$\mathcal{C} = \left\{ I^{(\text{su})}(j) \geq I_{\text{T}}^{(\text{su})}, j = 1, \dots, N_{\text{cand}} \right\} \quad (17)$$

and the non-detections

$$\mathcal{N} = \left\{ I^{(\text{su})}(j) < I_{\text{T}}^{(\text{su})}, j = 1, \dots, N_{\text{su}} - N_{\text{cand}} \right\}, \quad (18)$$

where  $N_{\text{su}} \equiv N_{\text{trials,noise}}$ . Further, assume that the direction for each candidate survey event is reobserved  $K_{\text{r}}$  times and that no signal is found above a threshold intensity  $I_{\text{T}}^{(\text{ro})}$ , yielding the set of non-detections during reobservations,

$$\mathcal{R} = \left\{ K_{\text{r}}(j) \times N_{\text{ch}}^{(\text{ro})} \text{ amplitudes} < I_{\text{T}}^{(\text{ro})}, j = 1, \dots, N_{\text{cand}} \right\}. \quad (19)$$

Because the total number of statistical tests in reobservations is much smaller than in the survey, the reobservation threshold may be significantly smaller than in the survey. For

simplicity in our discussion, we assume the threshold of all reobservations to be the same, but this need not be the case. It is a simple matter to account for thresholds that vary due to use of different dwell times or different background noise levels.

We distinguish reobservations where the scintillation gain is correlated with the gain,  $g_c$ , during the original candidate detection from those where it was uncorrelated. In practice, without explicit detection of an ETI signal over a sustained time, one does not know how long the gain is correlated because it depends on the strength of scattering to the particular source. Nonetheless, statistical inference from a set of observations (viz. an initial detection with only upper bounds in reobservations, as in META) depends on the degree of correlation assumed. We will make the simplifying assumption that reobservations have either *completely* correlated or completely uncorrelated gains. Consequently, we write the number of reobservations as the sum of correlated and uncorrelated numbers,

$$K_r(j) = K_{r,c}(j) + K_{r,u}(j). \quad (20)$$

The likelihood function for a given, *individual* candidate event is

$$\mathcal{L} = \mathcal{L}^{(\text{su})} \mathcal{L}^{(\text{ro})}, \quad (21)$$

where  $\mathcal{L}^{(\text{su})}$  is proportional to the probability density evaluated at the event's survey amplitude  $I^{(\text{su})}$  and  $\mathcal{L}^{(\text{ro})}$  is the probability that no detection was made in reobservations. For the three models presented in §5.1, the survey likelihoods are (dropping the  $j$  subscript for clarity)

$$\begin{aligned} \mathcal{L}_I^{(\text{su})} &\approx \Delta I f_I \left( I^{(\text{su})}; S = 0 \right) \\ \mathcal{L}_{\text{II}}^{(\text{su})} &\approx \Delta I f_I \left( I^{(\text{su})}; g_c S \right) \\ \mathcal{L}_{\text{III}}^{(\text{su})} &\approx \Delta I f_I \left( I^{(\text{su})}; S_{\text{RFI}} \right), \end{aligned} \quad (22)$$

where  $f_I$  is defined in §2.3 and Appendix B;  $\Delta I \ll I^{(\text{su})}$  is the uncertainty in establishing the survey amplitudes and  $g_c$  is the scintillation gain *at the time of the candidate detection*. The approximate equalities in Eq. 23 result because the exact form would be integrals over intensity of  $f_I$  over intervals  $\Delta I$  centered on the candidate intensity. The reobservation likelihoods are the probabilities of no detections in  $K_r$  reobservation trials:

$$\begin{aligned} \mathcal{L}_I^{(\text{ro})} &= \left[ 1 - P_d \left( I_T^{(\text{ro})}, 0 \right) \right]^{K_r} \\ \mathcal{L}_{\text{II}}^{(\text{cro})} &= \left[ 1 - P_d \left( I_T^{(\text{ro})}, g_c S \right) \right]^{K_{r,c}} \end{aligned} \quad (23)$$

$$\mathcal{L}_{\text{II}}^{(\text{uro})} = \left[ 1 - P_{d,\text{scint}} \left( I_T^{(\text{ro})}, S \right) \right]^{K_{r,u}} \quad (24)$$

$$\mathcal{L}_{\text{III}}^{(\text{ro})} = \left[ 1 - P_d \left( I_T^{(\text{ro})}, 0 \right) \right]^{K_r}.$$

Detection probabilities were introduced in §2.3 and Appendix B.

For Model II, we have written separate, reobservation likelihood functions for correlated and uncorrelated scintillation gains. It is useful to normalize intensities, thresholds, and signal strengths by the mean noise level  $\langle N \rangle$ , e.g.,

$$\begin{aligned}\eta &= I/\langle N \rangle \\ \zeta &= S/\langle N \rangle.\end{aligned}\tag{25}$$

The likelihood functions become

$$\begin{aligned}\mathcal{L}_I &= \mathcal{L}_I^{(\text{su})} \mathcal{L}_I^{(\text{ro})} = e^{-\eta} \left[ 1 - e^{-\eta_T^{(\text{ro})}} \right]^{K_r} \\ \mathcal{L}_{II} &= \mathcal{L}_{II}^{(\text{su})} \mathcal{L}_{II}^{(\text{ro})} = I_0 \left( 2\sqrt{\eta g \zeta} \right) e^{-(\eta+g\zeta)} \left[ 1 - P_d \left( \eta_T^{(\text{ro})}, g_c S \right) \right]^{K_{r,c}} \left[ 1 - e^{-\eta_T^{(\text{ro})}/(\zeta+1)} \right]^{K_{r,u}} \\ \mathcal{L}_{III} &= \mathcal{L}_{III}^{(\text{su})} \mathcal{L}_{III}^{(\text{ro})} = I_0 \left( 2\sqrt{\eta \zeta_{\text{RFI}}} \right) e^{-(\eta+\zeta_{\text{RFI}})} \left[ 1 - e^{-\eta_T^{(\text{ro})}} \right]^{K_r},\end{aligned}\tag{26}$$

where  $I_0$  is the Bessel function and we have dropped a (constant) factor  $(\Delta I/\langle N \rangle)$  on the right-hand side of each equation.

## 7. INDIVIDUAL CANDIDATE EVENTS WITH NO CORRELATED REOBSERVATIONS

In the surveys summarized earlier, unexplained, extrastatistical events are found in a few directions that, when reobserved, yield no evidence for persistent signals.

Here, we consider multiple reobservations of a given sky position (i.e., an *individual* candidate source) that are completely statistically independent. For the case of scintillating sources, this means that reobservations are made more than one scintillation time after an initial detection. While the META survey did, in fact, make “prompt” reobservations only 40 s after initial candidates were found, it is useful, for pedagogical reasons and for purposes of generality, to analyze events as if they were statistically independent. It is possible, for example, that the reobservations are, in fact, statistically independent if ETI sources are rare and are at large distances, thus producing short scintillation times (i.e.,  $\lesssim 40$  s). Moreover, we show in §8 that correlated reobservations combined with uncorrelated ones do not change substantially the conclusions we find here. In §9.2 we apply a likelihood analysis to an entire survey, which allows constraints to be made on the overall population of ETI transmitters that may exist in the Galaxy.

### 7.1. Comparison of Likelihood Functions for Individual Events

Some initial conclusions may be made from direct inspection of the likelihood functions. Firstly, given that survey events necessarily have large amplitudes (above the false-alarm threshold and, thus, well above the mean noise level  $\langle N \rangle$ ), the noise-only Model I has a low likelihood compared to the other two models. This becomes clear for events  $\eta \geq \eta_T \gg 1$  when we approximate  $I_0(x) \sim e^x/\sqrt{2\pi x}$  and calculate the ratio (dropping the ‘RFI’ subscript on  $\zeta$ ):

$$\frac{\mathcal{L}_{\text{III}}}{\mathcal{L}_{\text{I}}} \sim \frac{\exp(2\sqrt{\eta\zeta} - \zeta)}{(4\pi\sqrt{\eta\zeta})^{1/2}}. \quad (27)$$

For signal strengths  $1 < \zeta \lesssim \eta$  and candidate strengths  $\eta \geq 32$ , we have  $\mathcal{L}_{\text{III}}/\mathcal{L}_{\text{II}} > 10^3$ . Similarly, Model II can be shown to be far more likely than Model I for many parameter values. In general, for  $\eta \sim \zeta_{\text{RFI}} \sim g_c \zeta \gg 1$  and  $g_c \gg 1$  we find that Models II and III are much more strongly preferred than Model I. For sufficiently small scintillation gains,  $g_c$ , however,  $\zeta$  can be large enough that the reobservation factor  $\mathcal{L}_{\text{II}}^{(\text{ro})}/\mathcal{L}_{\text{I}}^{(\text{ro})}$  will make Model II less likely than even Model I.

Secondly, if we hypothesize, in Models II and III, that a strong source (real or RFI) underlies the event and that, whatever its nature, the amplitude was the same in either model (i.e.,  $g_c \zeta = \zeta_{\text{RFI}}$ ), then  $\mathcal{L}_{\text{II}}^{(\text{su})} \equiv \mathcal{L}_{\text{III}}^{(\text{su})}$ , but the net likelihood ratio is (assuming only uncorrelated reobservations for model II)

$$r \equiv \frac{\mathcal{L}_{\text{II}}}{\mathcal{L}_{\text{III}}} = \frac{\mathcal{L}_{\text{II}}^{(\text{ro})}}{\mathcal{L}_{\text{III}}^{(\text{ro})}} = \left[ \frac{1 - e^{-\eta_T^{(\text{ro})}/(\zeta+1)}}{1 - e^{-\eta_T^{(\text{ro})}}} \right]^{K_{r,u}} \leq 1. \quad (28)$$

The larger any real signal of average, continuous strength  $\zeta$  is in Model II, the smaller the likelihood ratio in Eq. 28 and the more that Model II is disfavored. However, if the survey detection was made when  $g_c$  was far out on the tail of the exponential pdf, then  $\zeta$  can be sufficiently small that  $\mathcal{L}_{\text{II}}/\mathcal{L}_{\text{III}} \rightarrow 1$ .

For a specified lower limit on  $r$ , e.g.,  $r \geq 0.5$ , one obtains a likely upper bound on  $\zeta$

$$\zeta \leq \zeta_{\text{max}} \equiv \frac{\eta_T^{(\text{ro})}}{\left| \ln \left[ 1 - r^{1/K_{r,u}} \left( 1 - e^{-\eta_T^{(\text{ro})}} \right) \right] \right|} - 1. \quad (29)$$

For  $K_{r,u} = 256$  (typical of META) and  $r \geq 0.5$ , we obtain  $\zeta \leq 2.38$  using a reobservation threshold of  $\eta_T^{(\text{ro})} = 20$ . For a typical candidate signal strength,  $\eta = 32$ , a scintillation gain  $g_c = \eta/\zeta \geq 13.4$  is required in the survey. The probability of this occurring is small,  $P_g(13.4) = e^{-13.4} = 10^{-5.8}$ , but it is large enough that in a many-trial survey, such a gain is likely to be encountered if  $N_{\text{trials, ISS}}$  is large, as discussed in §5.3.

Therefore, with measurements such as those outlined in §6, it is impossible to favor Model II over Model III. While  $P_g(13.4) = 10^{-5.8}$  is not large, given that we do not know the number of transmitters in the Galaxy and what  $g_{\max}$  might have been in the survey, we also cannot favor Model III over Model II. Statistically, over a set of events, however, it may be possible to conclude that an unlikely ensemble of scintillation gains is required to account for the known events. Also, the likelihood does not automatically account for the probability that particular scintillation gains will occur. For this reason, we extend our analysis in the next section to include Bayesian factors.

## 7.2. Bayesian Analysis of Individual Events

In this section we adopt a Bayesian analysis for the *a posteriori* joint pdf of  $g_c$  and  $\zeta$  for a particular candidate event. The Bayesian analysis proceeds by deriving a *a posteriori* pdf’s for the unknown parameters  $g_c, \zeta, \zeta_{\text{RFI}}$  by taking the product of the appropriate likelihood function (for a given model) with *prior* pdfs for the parameters and normalizing by the integral of the product over the parameter space. The advantage of this analysis is that it penalizes improbably large scintillation gains and large source fluxes.

The *a posteriori* pdf for a vector of parameters  $\boldsymbol{\theta}$  is, in terms of the survey detection with amplitude  $\eta_c$  and nondetections in reobservations,

$$f(\boldsymbol{\theta}|\eta_c\mathcal{I}) = \frac{f_{\boldsymbol{\theta}}(\boldsymbol{\theta})\mathcal{L}(\eta_c|\boldsymbol{\theta}\mathcal{I})}{f(\eta_c|\mathcal{I})}, \quad (30)$$

where  $\mathcal{L}$  represents one of the likelihood functions defined previously<sup>3</sup>;  $f_{\boldsymbol{\theta}}(\boldsymbol{\theta})$  is the joint *a priori* pdf for the parameters  $\boldsymbol{\theta}$ ;  $\mathcal{I}$  represents background information; and the denominator

$$f(\eta_c|\mathcal{I}) \equiv \int d\boldsymbol{\theta} f_{\boldsymbol{\theta}}(\boldsymbol{\theta})\mathcal{L}(\eta_c|\boldsymbol{\theta}\mathcal{I}) \quad (31)$$

normalizes the pdf.

Model I for candidate events (noise only) has no parameters other than the background noise level, which we assume to be known.

---

<sup>3</sup> Following standard practice, we explicitly show the background information as an element of the analysis. However, nonstandardly, we use “pdf” notation for the *posterior* and *prior* pdfs for the parameters rather than using the common, but misleading,  $p$  notation. We also write the likelihood function with arguments that often are written only when the identical quantity is referred to as the sampling distribution (e.g., Gregory & Loredó 1992).

In Model II, the two parameters to be determined for each event are the scintillation gain,  $g_c$ , and the intrinsic (average) signal strength,  $\zeta$ . We assume  $g_c$  and  $\zeta$  are statistically independent in the joint *prior* pdf, which therefore factors into the individual pdf's. The *prior* pdf for  $g_c$  is  $f_g(g_c) = \exp(-g_c)$ , appropriate for the strong scattering regime, which we assume. For  $\zeta$  (i.e.,  $S$ ) we adopt a pdf that corresponds to the power-law distribution of sources considered in §3.2 (cf. Eq. 9). We assume a Galactic disk population of sources ( $\alpha = 2$ ) and take the range of source strengths to be large,  $\zeta_1 \gg \zeta_0$  (or  $S_1 \gg S_0$ ). The *prior* pdf for  $\zeta$  is then

$$f_\zeta(\zeta) \approx \zeta_0 \zeta^{-2} U(\zeta - \zeta_0) U(\zeta_1 - \zeta) \quad (32)$$

where we have used Heaviside functions  $U$  to define the cutoffs of the power-law pdf.

The *posterior* pdf for Model II then becomes

$$f_{\text{II}}(g_c, \zeta | \eta_c \mathcal{I}) = \frac{f_g(g_c) f_\zeta(\zeta) \mathcal{L}_{\text{II}}(\eta_c | g \zeta \mathcal{I})}{f(\eta_c | \mathcal{I})}. \quad (33)$$

For the assumed *prior* pdfs (and dropping the Heaviside functions for clarity), we have

$$f_{\text{II}}(g_c, \zeta | \eta_c \mathcal{I}) \propto e^{-(g_c + g_c \zeta + \eta_c)} \zeta^{-2} I_0 \left( 2\sqrt{g_c \zeta \eta_c} \right) \left[ 1 - e^{-\eta_{\text{T}}^{(\text{ro})}/(1+\zeta)} \right]^{K_{\text{r,u}}}, \quad (34)$$

where the proportionality constant is  $\zeta_0/f(\eta_c|\mathcal{I})$ . Strictly, the cutoffs  $\zeta_{0,1}$  of the source strength distribution are also parameters to be estimated or constrained and they could be included explicitly in the *posterior* pdf, necessitating inclusion of corresponding *prior* pdfs on the right hand side of Eq. 33–34. For now, however, we treat these as hidden parameters, assuming that the range of source strengths,  $\zeta_0 \leq \zeta \leq \zeta_1$ , is large enough to include the best fit values of  $g_c$  and  $\zeta$ .

For Model III, which considers candidate events in the survey to arise from events that are intrinsically transient, we hypothesize a distribution of RFI amplitudes,  $f_{\text{RFI}}(\zeta_{\text{RFI}})$ , that has parameters to be determined via application of Bayes' theorem. As an illustration, we consider the simple example of a pdf that is constant in the interval  $\zeta_{0,\text{RFI}} = 0 \leq \zeta_{\text{RFI}} \leq \zeta_{1,\text{RFI}}$ ,

$$f_{\text{RFI}}(\zeta_{\text{RFI}}) = \frac{1}{\zeta_{1,\text{RFI}}} U(\zeta_{\text{RFI}}) U(\zeta_{1,\text{RFI}} - \zeta_{\text{RFI}}). \quad (35)$$

With the exception of multiplying constants, the resulting *posteriori* distribution does not differ from  $\mathcal{L}_{\text{III}}$ .

### 7.2.1. Application to META

Of the candidates reported by HS93, the majority of the extrastatistical events are near  $\eta_c = 32$  with a few at larger  $\eta_c$ . In Fig. 5 we show contours of the *posterior* pdf, Eq. 34, for four cases:  $\eta_c = 32$  and 100 with thresholds  $\eta_T^{(\text{ro})} = 10$  and 20; in all cases we assume that  $K_{r,u} = 256$  reobservations were attempted.

Table 2 displays the values of  $g_c$  and  $\zeta$  that maximize the *posterior* pdf for the specific  $\eta_c$  and  $\eta_T^{(\text{ro})}$  we have considered here. In general, we find that as  $\eta_c$  increases (for constant  $\eta_T^{(\text{ro})}$ ), the peak value of the pdf decreases, the region of constant probability becomes more concentrated about the peak, and the peak moves to larger gain and slightly larger signal strength.

A significant outcome of this analysis is that, at the time of the initial detection, the *apparent source strength*,  $g_c\zeta$ , is only about 50% of the measured candidate strength. The implication is that, even at these large intensities, the noise contributes significantly and sources with intrinsic intensities well below threshold will most likely be seen as the *combination* of a large scintillation gain and a large noise spike. Although large, the scintillation gains derived here are considerably less than those derived in our earlier discussion of the likelihood functions for Models II and III (cf. §7.1) where an observed intensity of  $\eta_c = 32$  implied a scintillation gain  $g_c \gtrsim 13.4$ . These smaller scintillation gains are considerably more probable,  $P(g \geq 6.2) = e^{-6.2} = 10^{-2.7}$ .

Figure 6 shows the best fit values for  $g_c$ ,  $\zeta$ , and  $g_c\zeta$  as a function of the number of uncorrelated reobservations,  $K_{r,u}$ . We show results for three values of the reobservation threshold,  $\eta_T^{(\text{ro})} = 5, 15, \text{ and } 20$ . In all cases, the product  $g_c\zeta$  is less than the apparent source strength at the time of the detection. This figure demonstrates two effects: (1) that noise *in general* plays a key role in producing candidate events in a large scale survey; and (2) even a large number of reobservations fails to constrain the source flux to be very small unless the reobservation threshold  $\eta_T^{(\text{ro})} \sim 5$ , much less than that used in META.

Our conclusions may be understood by referring to the various factors in Eq. 34. For event amplitudes ( $\eta_c$ ) of interest, the argument of the Bessel function is large,  $2\sqrt{g_c\zeta\eta_c} \gg 1$ . Using the large-argument approximation for  $I_0$ , we may write the *posterior* pdf for  $g_c$  and  $\zeta$  as

$$f_{\text{II}}(g_c, \zeta | \eta \mathcal{I}) \propto [e^{-g_c}] [\zeta^{-2}] \left[ e^{-\left(\sqrt{\eta_c} - \sqrt{g_c\zeta}\right)^2} (\eta_c g_c \zeta)^{-1/4} \right] \left[ 1 - e^{-\eta_T^{(\text{ro})}/(1+\zeta)} \right]^{K_{r,u}}. \quad (36)$$

The third and fourth bracketed factors in Eq. 36 represent the likelihood function  $\mathcal{L}_{\text{II}}$  and, by themselves, are maximized for  $g_c\zeta \sim \eta_c$  and  $\zeta \ll 1$ , respectively. Maximizing the



*likelihood function* therefore yields an apparent source flux  $g_c\zeta$  that is nearly equal to the observed candidate event  $\eta_c$  but favors actual source strengths  $\zeta$  that are small; hence, the ML value for  $g_c$  is large. The ML estimate for  $g_c$  is unrealistic because it is unlikely to have occurred in the number of trials considered, unless ETI is hyperabundant in the Galaxy. The Bayesian estimation procedure is far more realistic because it builds in penalties for both large scintillation gains and strong sources via the first two factors in Eq. 36. These factors favor, respectively, small  $g_c$  and small  $\zeta$ . We then see that it is through these two factors that the Bayesian estimates yield apparent source fluxes that are considerably smaller than the measured event amplitude.

The *a posteriori* pdf also displays, for small  $\eta_T^{(\text{ro})}$ , an important bimodality, as seen in Fig. 5c. One mode occurs at “large”  $g_c$  and  $\zeta$ ,  $g_c > 1$  and  $\zeta > 1$ , the other at the origin of the contour plot. The bimodality occurs once the number of reobservations  $K_{r,u}$  becomes large enough that the fourth factor in Eq. 36 compensates the third factor. For still larger  $K_{r,u}$ , the reobservation factor dominates and only the maximum near the plot origin remains. This “collapse” of the posterior pdf is a consequence of the particular source strength distribution,  $f_S(S)$ , we have adopted, namely a disk population of standard candles, which favors  $\zeta \rightarrow 0$  once the fourth factor dominates the third factor. In practice, we search for the maximum of  $f_{\text{II}}(g_c, \zeta | \eta \mathcal{I})$  with a minimum  $\zeta > 0$ ; for Fig. 5, we have searched  $\zeta \geq 0.1$ .

### 7.3. A Critical Number of Reobservations

The bimodal form of the *posterior* pdf in Eq. 34 may be used to derive the number of reobservations needed to rule out Model II, where the source strength,  $\zeta$ , is assumed constant in time. For META parameters, we have seen in the previous section that a small number of reobservations influences the parameter estimates for  $g_c$  and  $\zeta$  but they do not rule out Model II. Since, in the limit  $\zeta \rightarrow 0$ , Model II becomes identical to Model I, our approach will be to estimate the number of reobservations,  $K_{r,u}$ , required to make  $\zeta \ll 1$  the most probably value for  $\zeta$ .

The logarithm of the *posterior* pdf, Eq. 34, is

$$\lambda_{\text{II}} = -g_c - 2 \ln \zeta + \ln f_I(\eta_c, g_c\zeta) + K_{r,u} \ln \left[ 1 - P_{\text{d,scint}} \left( \eta_T^{(\text{ro})}, \zeta \right) \right]. \quad (37)$$

For the case where there are no reobservations ( $K_{r,u} = 0$ ),  $\lambda_{\text{II}}$  is maximized for  $g_c = 2$  and  $\zeta = \eta_c/2 - 9/4$ . The difference between  $\max(\lambda_{\text{II}})$  and its value for small signal strength,  $\zeta \lesssim 1$ , is  $\sim \eta_c$ . For reobservations to affect the location of the maximum significantly, the last term in Eq. 37, which favors small  $\zeta$ , must alter the slope  $\partial\lambda_{\text{II}}/\partial\zeta$  so that it becomes

negative for all  $\zeta \gtrsim 1$ . For such negative slopes, there cannot be a “large”  $\zeta$  maximum in  $\lambda_{\text{II}}$  that would imply a real signal was present. By maximizing  $\lambda_{\text{II}}$  with respect to  $g_c$  and requiring a negative slope at  $\zeta = 1$ , we obtain the number of reobservations needed to rule out a detectable signal. The result is  $K_{r,u} \geq [K_{r,u}]_{\text{crit}}$  where the critical number of reservations is, approximately, for  $\eta_c \gg 1$ ,

$$[K_{r,u}]_{\text{crit}} \approx \left[ \frac{\partial}{\partial \zeta} \ln(1 - P_{d,\text{scint}}) \right]^{-1} \left( \frac{\eta_c - 9}{4} \right) \approx \frac{e^{\eta_{\text{T}}^{(\text{ro})}/2}}{\eta_{\text{T}}^{(\text{ro})}} \left( 1 - e^{-\eta_{\text{T}}^{(\text{ro})}/2} \right) (\eta_c - 9). \quad (38)$$

In Fig. 7 we show  $[K_{r,u}]_{\text{crit}}$  plotted against the reobservation threshold  $\eta_{\text{T}}^{(\text{ro})}$  for several values of candidate strength  $\eta_c$ . The figure demonstrates that large thresholds produce exponentially large numbers of reobservations required to rule out Model II. For META, where a reobservation threshold  $\eta_{\text{T}}^{(\text{ro})} \approx 20$  was used,  $[K_{r,u}]_{\text{crit}} \approx 10^{4.3}$  for candidate events just above the survey threshold,  $\eta_{\text{T}}^{(\text{su})} = 31.7$ . Stronger candidate events require a greater number of reobservations.

*We conclude that candidate events in META cannot be ruled out as being due to scintillating sources, even if they transmit with constant power aimed into our direction, because there were too few reobservations and the threshold was too high.*

We also conclude that constraining reobservations must be made at lower thresholds than have been used (cf. Fig. 3). However, a lower reobservation threshold yields a larger number of false alarms. The false-alarm probability in reobservations is  $\exp[-\eta_{\text{T}}^{(\text{ro})}]$ . The number of false alarms expected in the critical number of reobservations (per frequency channel) is

$$\Delta N_{\text{fa}} = [K_{r,u}]_{\text{crit}} P_{\text{fa}}^{(\text{ro})} = \frac{e^{-\eta_{\text{T}}^{(\text{ro})}/2}}{\eta_{\text{T}}^{(\text{ro})}} \left( 1 - e^{\eta_{\text{T}}^{(\text{ro})}} \right) (\eta_c - 9). \quad (39)$$

Figure 7 also shows  $\Delta N_{\text{fa}}$  plotted against reobservation threshold. The dashed line shows where one false alarm is expected per frequency channel. For  $\eta_c = 32$  and  $\eta_{\text{T}}^{(\text{ro})} = 5$ ,  $\Delta N_{\text{fa}} \approx 0.38$ . While this number is small on a *per-channel* basis, when combined with the fact that reobservations need to search in frequency space to take into account unknown doppler shifts, it suggests that many false alarms are to be expected in reobservations made at small, otherwise constraining thresholds.

## 8. INDIVIDUAL CANDIDATE EVENTS WITH CORRELATED REOBSERVATIONS

In §7.2 the Bayesian estimates for scintillation gain  $g_c$  and source strength  $\zeta$  for individual events were made while assuming that the scintillation gain had decorrelated completely at the reobservation times. This corresponds to reobservations that are made hours or perhaps even just minutes after an initial detection. In META, however, a few reobservations were made within 40 s of the initial detection, a time short enough that the scintillations could have been highly, if not perfectly, correlated between the first few reobservations and candidate detection. In this section we consider such prompt, correlated reobservations in the Bayesian estimate of signal parameters in the context of Model II.

We assume, as before, that a candidate signal with amplitude,  $\eta_c$ , is reobserved in  $K_{r,u}$  unsuccessful trials where the scintillations are uncorrelated. In addition, we include  $K_{r,c}$  reobservations, also unsuccessful, where the scintillations are correlated over the time spanning the reobservations and the initial detection. To illustrate the effects of such correlated reobservations, we assume they are 100% correlated. In reality, the degree of correlation would vary slowly from 100% to zero correlation. But the point here is to demonstrate the stronger influence of perfectly correlated reobservations. We find, in fact, that the Bayesian estimates for  $g_c$  and  $\zeta$  are quantitatively different when correlated observations are included. However, the same conclusion is reached as before: the candidate events occur (if Model II is assumed) because noise and signal conspire to produce a threshold crossing in the survey. Moreover, though the number of uncorrelated reobservations needed to rule out Model II decreases when one or more correlated reobservations is made, the required number is still rather large unless smaller-than-used thresholds are used in the reobservations.

Unsuccessful, correlated observations introduce a new factor in the likelihood function and a *posteriori* pdf (cf. Eq. 33–34),  $[1 - P_d(I_T^{(ro)}, g_c\zeta)]^{K_{r,c}}$  or, equivalently, a term in the log pdf,

$$\lambda_{II}^{(cro)} = K_{r,c} \ln [1 - P_d(I_T^{(ro)}, g_c\zeta)]. \quad (40)$$

This term favors small values of  $g_c\zeta$ . When included with the other factors in the *posterior* pdf, it pushes estimates for  $g_c\zeta$  to values that are *lower* than if there were no correlated observations. The influence of correlated reobservations is illustrated in Fig. 8 (cf. Fig. 6), where estimates for  $g_c$ ,  $\zeta$ , and  $g_c\zeta$  are plotted against  $K_{r,u}$ , for several values of  $K_{r,c}$ , with thresholds  $\eta_T^{(ro)} = 20, 10, \text{ and } 5$ . The effects of the  $\lambda_{II}^{(cro)}$  term are to decrease the best fit  $\zeta$  as  $K_{r,c}$  increases. Also, the critical number of uncorrelated reobservations needed to favor  $\zeta \ll 1$  decreases as  $K_{r,c}$  increases. For the larger reobservation thresholds,  $\eta_T^{(ro)} = 20$  and 10, the necessary number of reobservations still measures in the hundreds, even for

$K_{r,c} = 16$  correlated reobservations. With the smaller threshold, only a few (but more than one) correlated reobservations cause the best fit  $\zeta$  to collapse below unity.

In Fig. 9, analogous to Fig. 7, we show the number of correlated reobservations needed to rule out Model II. Not surprisingly, this number is substantially smaller than the number of correlated reobservations. In practice, of course, the scintillation time scale limits how many correlated observations may be done. A general expression for the number of uncorrelated and correlated reobservations needed to rule out Model II is

$$\frac{\partial}{\partial \zeta} [P_{d,\text{scint}}^{K_{r,u}} + P_d^{K_{r,c}}]_{\zeta=1, g \sim \eta_c/4} > \left(\frac{\eta_c - 9}{4}\right). \quad (41)$$

We conclude that:

1. correlated but unsuccessful reobservations reduce estimates for  $g_c$  and  $\zeta$  from those seen in Fig. 6 where only uncorrelated reobservations were assumed;
2. the occurrence of unsuccessful, correlated reobservations does not obviate the conclusion that initial survey detections result from a noise-scintillation conspiracy where both noise and signal are needed to provide the survey detection; and
3. the noise-scintillation conspiracy makes it unlikely to detect the signal in a small number of reobservations.

## 9. GLOBAL ANALYSIS ON ENTIRE SURVEYS

In this section we return to the question we raised in §7.1: Although radiometer noise alone cannot explain the extrastatistical events seen in META and similar surveys, how likely is the scintillation interpretation? Restated, is the required *ensemble* of scintillation gains consistent with the gain pdf *and* with a plausible distribution of intrinsic source strengths?

### 9.1. Survey Intensity Distribution

As in §7, we take  $N_{\text{cand}}$  to be the number of candidate signals, i.e., those intensities above threshold, in the survey with the signal intensities in the set  $\mathcal{C}$  (cf. Eq. 17). These intensities are archived while the remaining  $N_{\text{su}} - N_{\text{cand}} \ll N_{\text{cand}}$  observations are discarded, so that the only information for these observations is that the intensity was less than  $I_{\text{T}}^{(\text{ro})}$ .

Now suppose that some fraction  $\epsilon_{\text{sky}}$  of the beam areas covered in the survey contain transmitting civilizations whose received signal strengths  $S$  (*before* accounting for scintillation modulations) are described by a pdf,  $f_S(S)$ , and that some fraction  $\epsilon_{\text{ch}}$  of the frequency channels surveyed contain power from broadcasting civilizations. In terms of previously defined quantities, we may write

$$\epsilon_{\text{sky}} = 1 - \langle e^{-N_b} \rangle, \quad (42)$$

where  $N_b$  is the average number of sources expected per beam (c.f. Eq. 3) and the exponential is averaged over all directions. The spectral fraction is

$$\epsilon_{\text{ch}} = \frac{N_{\text{signals/beam}} \Delta\nu_{\text{spectrometer}}}{B_D N_{\text{ch}}} \lesssim \frac{N_{\text{signals/beam}}}{N_{\text{ch}}}, \quad (43)$$

where  $N_{\text{signals/beam}} = N_{\text{lines}} \langle N_b \rangle$ , with  $\langle N_b \rangle$  being the number of sources in a telescope beam, averaged over all directions. The total fraction of sources contained in the  $N_{\text{su}}$  survey “cells” is given by  $\epsilon_{\text{su}} = \epsilon_{\text{sky}} \epsilon_{\text{ch}}$ .

The fraction  $\epsilon_{\text{sky}}$  can be related to the number density of sources  $n_D$  defined in §3.1 As we show in that section, even a small number of transmitting civilizations,  $\approx 10^3$ , can result in more than one source per beam so that  $\epsilon_{\text{sky}}$  need not be small and may in fact approach unity. However, it is assumed that transmitting civilizations will use narrow bandwidths,  $\lesssim 1$  Hz, in a small number of individual channels. Since the center frequencies of such narrowband signals are not known *a priori*, it is obviously necessary to cover as large a range in frequency as possible in the survey, necessitating that the number of channels,  $N_{\text{ch}}$ , be quite large (e.g., in META,  $N_{\text{ch}} \approx 10^7$ ). Consequently, we expect  $\epsilon_{\text{su}} \lesssim \epsilon_{\text{ch}} \ll 1$ .

Within the context of the three models presented in §§5–6, the sampling pdf for the candidate intensities is

$$\begin{aligned} f_I^{(\text{su})}(I) &= (1 - \epsilon_{\text{su}} - \epsilon_{\text{RFI}}) f_I(I, S = 0) \\ &+ \epsilon_{\text{su}} \int dS f_S(S) f_{I,\text{scint}}(I, S) \\ &+ \epsilon_{\text{RFI}} \int dS f_{\text{RFI}}(S_{\text{RFI}}) f_I(I, S_{\text{RFI}}). \end{aligned} \quad (44)$$

Here the first term accounts for observation cells devoid of sources, the second term accounts for those cells with scintillating sources, and the third term accounts for transient sources. Analogous to  $\epsilon_{\text{su}}$ , we have introduced  $\epsilon_{\text{RFI}}$ , the fraction of observation cells in which there is a transient signal. Just as  $\epsilon_{\text{su}}$  can be related to the number of transmitters in the Galaxy, the rate at which transient signals occur and their duration can be related to  $\epsilon_{\text{RFI}}$ .

Following §6 we use likelihood functions involving  $f_I^{(\text{su})}$  to test various models. Our goal is to test the hypothesis that a population of scintillating sources can account for some

of the events seen in SETI programs and to estimate parameters of any such population. Accordingly, we shall consider the same models as in §6: a population of scintillating sources, Model II, for which  $\epsilon_{\text{RFI}} = 0$ , and an RFI-only explanation for the events, Model III, for which  $\epsilon_{\text{su}} = 0$ . However, should there be a method of distinguishing between terrestrial RFI and narrowband celestial transients in the future, our analysis can easily be extended to include such possibilities.

We shall also need the detection probability for the survey. Integrating Eq. 44, we have

$$P_{\text{d}}^{(\text{su})} = (1 - \epsilon_{\text{su}})P_{\text{fa}}^{(\text{su})} + \epsilon_{\text{su}} \int dS f_S(S) P_{\text{d,scint}}(I_{\text{T}}^{(\text{su})}, S), \quad (45)$$

for Model II; for Model III, a similar expression holds with the substitution of  $\epsilon_{\text{RFI}}$  for  $\epsilon_{\text{su}}$  and  $P_{\text{d}}(I_{\text{T}}^{(\text{su})}, S)$  for  $P_{\text{d,scint}}(I_{\text{T}}^{(\text{su})}, S)$ . Here,  $P_{\text{fa}}^{(\text{su})}$  refers to the false-alarm probability for the survey as a whole, hence,  $N_{\text{su}}P_{\text{fa}}^{(\text{su})} \sim 1$ . We expect

$$\langle N_{\text{cand}}^{(\text{su})} \rangle = N_{\text{su}}P_{\text{d}}^{(\text{su})} \quad (46)$$

to be the expected number of candidate signals found in the survey. If there is noise only, amplitudes will follow the exponential pdf that results from Eq. B4 with  $S = 0$ .

In practice, the noise level  $\langle N \rangle$  is not constant over all sky positions, due to ground spillover and Galactic latitude dependent backgrounds. A survey may be divided into regions where  $\langle N \rangle$  is constant and each region can be analyzed individually. Here, however, since our goal is to exemplify a method of inference, we assume  $\langle N \rangle$  to be constant.

## 9.2. Likelihood Function for the Entire Survey

The likelihood function for the survey is

$$\mathcal{L}^{(\text{su})} = \mathcal{L}_{\text{cand}}\mathcal{L}_{\text{non}}, \quad (47)$$

where the factor for survey candidates is

$$\mathcal{L}_{\text{cand}} = \prod_{j=1}^{N_{\text{cand}}} f_I^{(\text{su})}(I_j) \quad (48)$$

and the non-detection factor is

$$\mathcal{L}_{\text{non}} = \prod_{j=1}^{N_{\text{su}} - N_{\text{cand}}} P(I < I_{\text{T}}^{(\text{su})}) = [1 - P_{\text{d}}^{(\text{su})}]^{N_{\text{su}} - N_{\text{cand}}}. \quad (49)$$

For our assumed form of  $f_I^{(\text{su})}$ , the parameters of interest are the fraction of survey cells containing sources or RFI,  $\epsilon_{\text{su}}$  and  $\epsilon_{\text{RFI}}$ , and the parameters of the source and RFI strength distributions,  $f_S(S)$  and  $f_{\text{RFI}}(S)$ .

As in our analysis of individual events in §7, we again assume that reobservations occur at times such that the scintillation gain is uncorrelated between all survey and reobservation measurements<sup>4</sup>. With  $K_r(j)$  reobservations per candidate, the likelihood function for the reobservations is

$$\mathcal{L}^{(\text{ro})} = \prod_{j=1}^{N_{\text{cand}}} \prod_{k=1}^{K_r(j)} P\left(I < I_T^{(\text{ro})}\right) = \left[1 - P_d^{(\text{ro})}\right]^{\sum_j^{N_{\text{cand}}} K_r(j)}. \quad (50)$$

Equivalent to the survey detection probability in Eq. 45 is a reobservation detection probability

$$P_d^{(\text{ro})} = (1 - \epsilon_{\text{ro}})P_{\text{fa}}^{(\text{ro})} + \epsilon_{\text{ro}} \int dS f_S(S) P_{\text{d,scint}}\left(I_T^{(\text{ro})}, S\right) \quad (51)$$

where we have distinguished, through the label “ro,” the false-alarm probability, the source-detection probability, the threshold, and the fraction of cells containing sources in the reobservations from those conducted in the survey observations. Reobservations have a lower threshold intensity,  $I_T^{(\text{ro})}$ , and, accordingly, larger false-alarm and detection probabilities. The beam fraction,  $\epsilon_{\text{sky}}^{(\text{ro})}$ , is also different from that in the survey because directions are selected in the survey that have shown strong signals. If there is a population of sources we would expect  $\epsilon_{\text{sky}}^{(\text{ro})} \rightarrow 1$ , but we still expect  $\epsilon_{\text{ch}}^{(\text{ro})} \ll 1$  and  $\epsilon_{\text{ro}} \lesssim \epsilon_{\text{ch}}^{(\text{ro})}$ . For instance, to cover a bandwidth equivalent to the Doppler shift resulting from the Earth’s motion,  $10^{-4}c$ , at an observing frequency of 1 GHz requires  $10^5$  channels of 1 Hz each. In this example, therefore,  $\epsilon_{\text{ch}}^{(\text{ro})} \sim 10^{-5}$ .

In our earlier analysis of the individual events, §7, we assumed that  $S_{\text{RFI}} = 0$  during reobservations. In contrast, since we are now analyzing the *entire* survey, we must allow for the possibility of RFI to be present during the reobservations. Consequently, in considering reobservations in Model III, we use Eq. (51) with the substitution  $P_d\left(I_T^{(\text{ro})}, S\right)$  in place of  $P_{\text{d,scint}}\left(I_T^{(\text{ro})}, S\right)$ .

The complete likelihood function is

$$\mathcal{L} = \mathcal{L}^{(\text{su})} \mathcal{L}^{(\text{ro})}. \quad (52)$$

In practice, we analyze the log likelihood,

$$\Lambda \equiv \log \mathcal{L} = \Lambda_{\text{cand}} + \Lambda_{\text{non}} + \Lambda_{\text{ro}}. \quad (53)$$

---

<sup>4</sup> Assumption of uncorrelated vs. correlated reobservations is not critical; reobservations of survey candidates are dominated by the vastly greater number of nondetections in the survey itself.

Parameter values may be estimated through maximization of  $\Lambda$ . Alternatively, Bayes' theorem may be applied by multiplying  $\mathcal{L}$  by a *prior* probability density for the parameters and normalizing to obtain the *posterior* pdf for the parameters. In the following we analyze only the likelihood function. This choice is made because (1) the pdfs for scintillation gain and source strength are already built into the likelihood function; and (2) any *prior* pdfs for the relevant parameters,  $\zeta_1$ ,  $\zeta_0$ ,  $\epsilon_{\text{su}}$ , and  $\epsilon_{\text{ro}}$ , would be so broad that they would not change the net results.

### 9.3. Fitting Model II to META

In Fig. 10*a* and *b* we show the likelihood functions for Model II at 1420 and 2840 MHz, respectively, using the META results (HS93). Table 3 reports the location and amplitude of the maximum in the likelihood function for both the survey and the survey plus reobservations of candidates. In column 1 is the radio frequency, column 2 is the maximum amplitude of the logarithm of the likelihood function, and columns 3 and 4 are the maximum likelihood values for  $\zeta_0\epsilon_{\text{su}}$  and  $\zeta_1$ , respectively. We do not present the results for  $\Lambda_{\text{cand}}$  or  $\Lambda_{\text{non}}$  because there exists no single maximum for these functions, but rather a region of constant and maximum likelihood.

There are several aspects of these results which deserve explanation. Horowitz & Sagan (1993) report 14 candidates at 1420 MHz and 23 candidates at 2840 MHz, all with intensities greater than  $28\langle N \rangle$ . However, they also acknowledge that they have included candidates just below threshold so as not to exclude potential sources. In producing these likelihood functions, we have used only those 11 candidates above the proper survey threshold,  $\eta_{\text{T}}^{(\text{su})} = 31.7$ . We have also assumed that all reobservations were conducted with a threshold of  $\eta_{\text{T}}^{(\text{ro})} = 20$  ( $P_{\text{fa}} = 10^{-8.7}$ ) and that each candidate was reobserved  $K_j = 256$  times. In order to continue plotting the likelihood functions as functions of only two parameters, we have set the ratio,  $r_\epsilon \equiv \epsilon_{\text{ro}}/\epsilon_{\text{su}}$ , to be constant and equal to unity. Finally, the likelihood function for Model II is plotted as a function of  $\zeta_0\epsilon_{\text{su}}$  and  $\zeta_1$ . The degeneracy between the parameters  $\zeta_0$  and  $\epsilon_{\text{su}}$  arises because  $f_S(S) \propto \zeta_0$ , cf. Eqs. 44, 45, and 51. In the limit  $\zeta_0 \ll 1$ , the quantities  $f_I^{(\text{su})}(I)$ ,  $P_{\text{d}}^{(\text{su})}$ , and  $P_{\text{d}}^{(\text{ro})}$  become approximately linear in the quantity  $\zeta_0\epsilon_{\text{su}}$ .

There is no difference in either the magnitude or location of the peak likelihood when comparing  $\Lambda_{\text{su}}$  and  $\Lambda_{\text{su+ro}}$ . The lack of the reobservations' influence arises because of the vastly larger number of nondetections in the original survey than reobservations. For the non-detections,

$$\Lambda_{\text{non}} \approx N_{\text{su}} \log \left[ 1 - P_{\text{d}}^{(\text{su})}(\eta_{\text{T}}^{(\text{su})}, \epsilon_{\text{su}}, \zeta_1) \right] \approx -N_{\text{su}} P_{\text{d}}^{(\text{su})}, \quad (54)$$



where we have used the expansion  $\log(1 - x) \approx -x$ . A similar expression holds for  $\Lambda_{\text{ro}}$ ,  $\Lambda_{\text{ro}} \approx -N_{\text{cand}} K_r P_d^{(\text{ro})}$ . These two likelihood functions have a similar shape in the  $(\zeta_0 \epsilon_{\text{su}}, \zeta_1)$  plane. However, because  $N_{\text{su}} \approx 10^{13}$  while  $N_{\text{cand}} K_r \approx 10^3$ , the nondetection likelihood completely dominates the influence of the reobservation likelihood.

Thus,  $\Lambda_{\text{su+ro}}$  is dominated by  $\Lambda_{\text{cand}}$  and  $\Lambda_{\text{non}}$ .  $\Lambda_{\text{cand}}$  increases (and  $\Lambda_{\text{non}}$  decreases) if either  $\zeta_0 \epsilon_{\text{su}}$  or  $\zeta_1$  (or both) increases, as a result of the larger number of sources that can be detected. When these two are combined to produce  $\Lambda_{\text{su+ro}}$ , the maximum of the likelihood function occurs at values for  $\zeta_0 \epsilon_{\text{su}}$  and  $\zeta_1$  that are intermediate to those which respectively maximize  $\Lambda_{\text{cand}}$  and  $\Lambda_{\text{non}}$ . As  $S_1$  is the *upper cutoff* to the source strength pdf, a simple constraint on  $\zeta_1$  is that it cannot be too much smaller than the intensity of the strongest candidate observed<sup>5</sup>. Similarly, given the small number of candidates (i.e., a few tens out of  $\sim 6 \times 10^{13}$  total trials), we would expect that  $\epsilon_{\text{su}}$  is small. The contours extending to very large  $\zeta_1$  arise, in part, because of the exponential pdf for the scintillation gain. Since the most probable gain is  $g = 0$ , very large  $\zeta_1$  can be tolerated and the absence of sources with  $\zeta \sim \zeta_1$  in the survey is explained by assuming that scintillations modulated any such sources below threshold.

The locations of the peaks at the two frequencies compare favorably. The location of the peak likelihood at 1420 MHz is within 10% of the peak likelihood at 2840 MHz and the 2840 MHz peak likelihood is within 50% of the 1420 MHz peak likelihood. The lack of better agreement can be attributed to the fact that there were twice as many 2840 MHz candidates as 1420 MHz candidates and the strongest 2840 MHz candidate had  $\eta = 746.6$  while the strongest 1420 MHz candidate had  $\eta = 224$ .

The difference in strongest candidate signals between the two frequencies would seemingly explain the difference in the amplitude of the likelihood functions as well. It does not. At 1420 MHz, there are four candidates, three with  $\eta \approx 34$  and one with  $\eta = 224$ . At 2840 MHz, there are seven candidates, three with  $\eta \approx 32$ , one at  $\eta = 746.6$ , and three with  $40 < \eta < 80$ . It is these last three candidates which cause the marked difference in the maximum value of the likelihood functions, simply because there are so many of them. An occasional large scintillation gain can combine with a large noise fluctuation (cf. §7.2.1) to produce a signal well above threshold. Hence, the likelihood function is somewhat insensitive to one candidate with an observed intensity well above threshold. However, obtaining several, independent combinations of such gains and noise fluctuations becomes increasingly, and rapidly, less likely.

---

<sup>5</sup>  $\zeta_1$  can be smaller than the intensity of an observed candidate by virtue of upwards noise and scintillation fluctuations.

#### 9.4. Fitting Model III to META

The above discussion implicitly assumes that Model II (a population of scintillating sources) is the correct model. To compare Model II with Model III (the RFI model), we have also constructed the likelihood functions for this model, Fig. 10*c* and *d*. The maxima and locations of the likelihood functions are tabulated in Table 3.

In estimating these likelihood functions, we have taken  $f_{\text{RFI}}$  to be a flat function, as in §7.2, with an upper limit  $S_{1,\text{RFI}}$  and a lower limit  $S_{0,\text{RFI}} = 0$ . As for Model II, we have assumed that each candidate position was reobserved 256 times and that  $r_\epsilon$  is constant and equal to unity.

The likelihood functions for Model III are very similar to those of Model II. Again  $\Lambda_{\text{su+ro}} \approx \Lambda_{\text{su}}$  because of the vastly larger number of survey observations;  $\Lambda_{\text{cand}}$  increases with increasing  $\epsilon_{\text{RFI}}$  and/or  $\zeta_{1,\text{RFI}}$  while  $\Lambda_{\text{non}}$  decreases, with the combination of these two producing a peak in  $\Lambda_{\text{su}}$ .

There are two notable differences between the likelihood functions for the two models, both arising from the assumed  $f_{\text{RFI}}$ . Since the pdf is flat, all intensities are equally likely, in contrast to Model II, where it is possible to “hide” very large intensities with a very small scintillation gain. Consequently, a smaller  $\epsilon_{\text{RFI}}$  is required for Model III than Model II in order that there not be too many candidates. Similarly, the peak likelihood tends to be more concentrated about the most likely  $\zeta_{1,\text{RFI}}$ , rather than extending to very large values as for Model II.

The key issue between these two models, though, is the value of the likelihood functions at the peak. At both frequencies, we find that the maximum likelihoods differ only slightly, with the RFI model slightly preferred at 1420 MHz and the scintillating source model slightly preferred at 2840 MHz. *We conclude that we are unable to favor either Model II or Model III.*

#### 9.5. Interpretation of Model II Fitting Results

The fitting results yield estimates for  $\zeta_0\epsilon_{\text{su}} = \zeta_0\epsilon_{\text{sky}}\epsilon_{\text{ch}}$  and  $\zeta_1$ , the normalized upper cutoff of the source flux pdf. Using results from §3 and Eq. (42)–(43), we may relate these estimated quantities to the population parameter  $N_{\text{D}}$ , the number of sources in the Galaxy. Figure 11 shows  $\epsilon_{\text{sky}}$  as a function of the mean free path (c.f. Eqs. [3] and [42]) for a simple disk model for the Galaxy. We have assumed a circular disk of radius  $R_{\text{G}} = 15$  kpc and thickness  $2H_{\text{G}} = 0.2$  kpc with the Sun at the disk center (heliocentricity for simplicity!).

From the fitting results we can derive two estimates for  $N_D$ , the number of sources in the Galaxy, in terms of the survey parameter,  $\epsilon_{\text{su}}$ . The first relation results from inverting the relation  $\epsilon_{\text{su}} = \epsilon_{\text{sky}}\epsilon_{\text{ch}}$  where  $\epsilon_{\text{sky}}$  is related to  $D_{\text{mfp}}$  (as in Fig. 11) which, in turn, is a function of  $N_D$ ,  $D_{\text{mfp}} \propto N_D^{-1/3}$ :

$$N_D^{(1)} = \epsilon_{\text{sky}}^{-1}(\epsilon_{\text{su}}N_{\text{ch}}/P_\nu), \quad (55)$$

where ‘ $\epsilon_{\text{sky}}^{-1}$ ’ means the inverse of the function  $\epsilon_{\text{sky}}(N_D)$  that relates the number of sources  $N_D$  to  $\epsilon_{\text{sky}}$ ;  $P_\nu$  is the probability that a signal is in the band observed by META. Here we define this probability as  $P_\nu = N_{\text{signals/beam}}\Delta\nu_{\text{spectrometer}}/B_D$ .

The second relation is based on the relationship between  $N_D$  and the flux ratio  $S_1/S_0 \equiv \zeta_1/\zeta_0$ . We can determine only  $\zeta_1$  and the product  $\zeta_0\epsilon_{\text{su}}$  from the likelihood analysis. Let the ratio of these fitting parameters be

$$F \equiv \frac{\zeta_1}{\zeta_0\epsilon_{\text{su}}}. \quad (56)$$

Inverting the ratio  $\zeta_1/\zeta_0$  (cf. §3.2 yields

$$N_D^{(2)} = \begin{cases} \frac{F\epsilon_{\text{su}}}{1 - F\epsilon_{\text{su}}/2\tilde{N}_D} & N_D^{(2)} \leq \tilde{N}_D \\ (F\epsilon_{\text{su}})^{3/2}\tilde{N}_D(H_G/R_G)^3 & N_D^{(2)} \geq \tilde{N}_D. \end{cases} \quad (57)$$

Figure 12 shows the two estimates for  $N_D$  plotted against  $\epsilon_{\text{su}}$  for  $P_\nu = 0.01$ . Increasing  $P_\nu$  shifts  $N_D^{(1)}$  (solid curve) to the right. Therefore, in order that there be a solution defined by the crossing points of the two curves,  $P_\nu$  must exceed a minimum of about 0.003. This would suggest that the total radio domain of ETI signals is about 300 times the META bandwidth if there is only one ETI transmitter per beam. But with more than one transmitter per beam, the spectral domain can exceed the META bandwidth by much more than this factor.

For values of  $P_\nu$  that provide solutions, the number of civilizations can be anywhere from a few to in excess of  $10^{10}$ . The reason for this indeterminacy is that, with larger  $\epsilon_{\text{su}}$ ,  $\zeta_0$  decreases. This implies, simply, that though there are many more sources for larger  $\epsilon_{\text{su}}$ , the vast majority is buried in the noise. Unfortunately, the ambiguity in  $N_D$  means we cannot establish, through this analysis, the distance scale for putative sources consistent with META candidates. Therefore we cannot constrain the transmitter power with the available information we have used.

Horowitz & Sagan point out that the strongest candidates in META cluster about the Galactic plane. We can use the spatial distribution to estimate the distance scale and thus

provide another constraint on  $N_{\text{D}}$ . For the uniform disk model of §3, and where sources can be detected above threshold out to a distance  $D_{\text{max}}$  with  $H_{\text{G}} \leq D_{\text{max}} \leq R_{\text{G}}$ , we have

$$\langle \sin^2 b \rangle = \frac{1}{3} \left( \frac{H_{\text{G}}}{D_{\text{max}}} \right)^3 \left( 1 + 3 \ln \frac{D_{\text{max}}}{H_{\text{G}}} \right). \quad (58)$$

From the nine strongest META candidates, we estimate  $\langle \sin^2 b \rangle \approx 0.097$  compared to a value  $1/3$  for an isotropic population, implying  $D_{\text{max}}/H_{\text{G}} \approx 2.3$ . The disk subvolume sampled by these nine events is  $V_9 = \frac{2\pi}{3} H_{\text{G}}^3 [3(D_{\text{max}}/H_{\text{G}})^2 - 1]$  out of a total volume  $V = 2\pi H_{\text{G}} R_{\text{G}}^2$ . For  $R_{\text{G}}/H_{\text{G}} = 150$ , as in §3, we find that  $V/V_9 \approx 10^{3.7}$ . Thus the nine events found in  $V_9$  imply the presence of  $N_{\text{D}} \approx 10^{4.6}$  sources in the Galaxy. This number is comparable to the cross-over point of the two lines in Figure 12.

We conclude that if the nine strongest META events are real celestial sources (natural or artificial), there are a few tens of thousands of such sources in the Galaxy.

## 10. DUAL STATION & DUAL BEAM OBSERVATIONS

Here we discuss the joint intensity statistics of SETI made simultaneously at two sites. Most of our discussion also applies to multiplying interferometry, such as proposed by Welch (1983). Simultaneous SETI observations at two terrestrial locations are analogous to pairs of single-site observations made at different times when one considers the level of correlation for the interstellar scintillations.

In Appendix B we discuss the spatial correlation of ISS. The correlation length is directly related to the scintillation time because the underlying process is a diffraction pattern swept across the line of sight at a transverse speed  $V_{\perp}$ . Referring to Fig. 1, scintillation times for nearby sources are measured in hours while much faster scintillations, with time scales of seconds, will be seen from sources across the Galaxy. Transverse speeds  $V_{\perp} \sim 10 \text{ km s}^{-1}$  then correspond to length scales ranging from tens of km to  $> 10^4 \text{ km}$ . Dual-site SETI observations will therefore encompass all possible degrees of correlation of the scintillation gain. These are (1) perfect correlation for nearby sources; (2) partial correlation for intermediate distances; and (3) no correlation for distant sources. At 1.4 GHz, sources within 1 kpc will show highly correlated scintillations for any pair of terrestrial sites and those at distances greater than 5–8 kpc will display uncorrelated gains for sites more than 1000 km apart. We emphasize that the relevant distances for demarcating these regimes are frequency dependent. At frequencies higher than 1.4 GHz, more sources in the Galaxy will show scintillations that are spatially correlated between two sites.

Dual-site observations are therefore equivalent, statistically, to single-site reobservations made promptly after an initial detection (such that ISS is strongly correlated) and those made with substantial time delay, in which case the ISS is uncorrelated. As we saw in §2.3, the probability of detecting an ETI signal in even a prompt reobservation need not be large and the probability of redetection in a delayed, uncorrelated reobservation can be negligible.

If  $N_{\text{trials,ISS}}$  is large (cf. Eq. 10), a survey is expected to encounter rare, high amplitude scintillations, in which case weak sources may be detected at one site as a combination of noise and signal with low chances of redetection (either later in time or at the other site). This conclusion restates our analysis of META events made in §7. Similarly, small  $N_{\text{trials,ISS}}$  means that only smallish scintillation gains are to be expected in a survey. In both cases, however, rare noise fluctuations play a key role in detections of sources because of the large number of noise trials.

We refer to the analysis of §2.3 on temporal sequences of observations to analyze dual-site observations. Figure 3 shows the detection probability of a second observation with threshold  $I_T$  given that a first observation was made that yielded an intensity  $I_1$ . The detection probability is plotted against the correlation coefficient  $\rho$  (which may be either the temporal or the spatial correlation). The results for the several values of  $I_T$  and  $0 \leq \rho \leq 1$  indicate that the probability of detection at a second site is small, even when  $\rho$  is large.

### 10.1. META & META II Two-station Observations

META and META II devote some observing time to simultaneous observations at 1.42 GHz and with a survey threshold  $\eta_T = 16$  at each site. For detections at threshold at one site, i.e.,  $\eta_1 = 16$ , Fig. 3 provides the detection probability for the other site. Even for large intrinsic signal strengths, e.g.,  $\zeta = 32$ , the chance of *not* detecting the source at the second site is non-negligible,  $\approx 35\%$ . If the initial detection was of a weak source, e.g.,  $\zeta \leq 4$ , modulated above threshold by a large scintillation gain or noise fluctuation or both, the probability of detecting the source at the second site can easily be less than 10%. In accord with our previous discussion, a significantly lower threshold (e.g.,  $10\langle N \rangle$ , c.f. Fig. 3 and §11) would make detections at both sites much more probable, albeit with a larger background false-alarm rate. Part of the task of subsequent processing would be an assessment of whether excess hits above the background rate were statistically significant (see §11).

## 10.2. Future Two-station or Dual-Beam Observations

The recommended procedure for dual-site observations is to report observations at low thresholds. This necessitates a large amount of storage for results in a dual-site search but raises the odds of a dual detection. As discussed in §11, there are additional reasons for reporting more measurements than are typically done in SETI.

In the proposed BETA survey, a billion channel spectrometer will be used in a two-feed antenna system so that a given sky position is viewed successively in the two beams (HS93). The time delay is of order minutes, so scintillating sources may or may not be correlated in the two beam measurements, depending on observation frequency and source distance. The odds for dual detections depend on the observing threshold according to our previous considerations, with lower thresholds preferred.

## 10.3. SETI Interferometry

Welch (1983) has emphasized the inferential power of multiplying interferometry in SETI with respect to localization on the sky and for establishing the celestial nature of any real sources by seeing the influence of the expected Doppler shifts. ISS influences interferometric observations by attenuating the visibility function by a factor  $\rho_s(b)$ , where  $b$  is the interferometer baseline.

# 11. ALTERNATIVE DETECTION METHODS

The conventional detection method in SETI and other astronomical surveys uses a threshold in signal-to-noise ratio (SNR) to define candidate signals. The false-alarm probability is often used to define the threshold in terms of the number of statistical trials made in the survey.

Here we advocate an alternative method for SETI that uses more information in the data and *a priori* knowledge about the noise statistics. This method allows lower signal levels to be probed than in the SNR method. The scheme, first discussed by Zepka, Cordes & Wasserman (1994) for detecting X-ray sources in Poisson backgrounds, looks for departures from the expected shape of the intensity (or count-rate) histogram. The stopping criterion is that sources are identified iteratively until the histogram of residual intensities is consistent with a noise-only histogram. For this reason, we refer to the method as “pdfCLEAN.”

For interference-free and source-free observations, the *a priori* intensity pdf is given in Eq. B4 with  $S = 0$ , and is a one-sided exponential,  $\exp(-\eta)$ . The histogram of intensities,  $h_k$ , is the number of counts in the  $k^{\text{th}}$  intensity bin with centroid value  $\eta_k$ . For  $N_{\text{obs}}$  total observations, the mean value of the histogram is

$$\langle h_k \rangle = N_{\text{obs}} \exp(-\eta_k). \quad (59)$$

The *actual* number of counts in  $h_k$  is a Poisson random variable such that the probability of obtaining  $h_k$  counts is given by

$$P(h_k) = \frac{e^{-\langle h_k \rangle} \langle h_k \rangle^{h_k}}{h_k!}. \quad (60)$$

Departures from the expected exponential shape are identified by seeking histogram bins where  $P(h_k)$  is small, indicating an excess or deficit of counts. The pdfCLEAN method therefore makes use of a *probability threshold* in place of an SNR threshold in the SNR method. Once histogram bins are found in this way, they may be “deconstructed” to find the original sky positions and frequency channels of the contributing intensities. These may then be subjected to clustering tests to see if real celestial signals or terrestrial interference is the cause for departure.

Application of pdfCLEAN requires substantial storage for raw data results because it can be used to probe intensities at lower SNR than can the SNR method itself. A discussion of actual storage requirements is given below. The payoff, however, is that real sources can be identified at low levels and the interference environment can be better understood as well. Zepka et al. (1994) show that the number of spurious detections (e.g., due to noise fluctuations) is small using pdfCLEAN.

## 12. RECOMMENDATIONS FOR FUTURE SETI PROGRAMS

Several lines of argument that we have presented lead to a primary recommendation for future SETI: *Signal detections should be reported at much lower signal levels than have been used.* In programs like META, where a large-scale survey is performed at one threshold with subsequent reobservations at a lower threshold, we argue that the reobservation threshold should be low enough to rule out our Model II where survey candidates are hypothesized to be scintillating but otherwise constant sources.

The cost of reporting lower signal levels is a larger recording rate and, possibly, a problematic level of false alarms. The latter is particularly the case if the candidate frequency is expected to vary between survey detection and reobservation, necessitating a

large number of frequency channels to be searched during the reobservations. However, in §11 we argue that false-alarms need not deter a survey from detecting weak sources. Use of the Zepka et al. (1994) pdfCLEAN method allows signals to be extracted from histogram counts that contain many noise-only measurements (i.e., false alarms).

To estimate the threshold to be used for recording spectral amplitudes, we consider the technological limits on practical data recording. At present, it is feasible to record approximately one high-density magnetic tape per day and expect to analyze it at approximately the real-time rate on a network of workstations. This is approximately 10 Gbytes/day. The data rate is

$$\dot{\beta}_{\max} = \frac{e^{-\eta_T} N_{\text{ch}} \beta}{T_s}, \quad (61)$$

and the corresponding threshold is

$$\eta_T = \ln \left[ \frac{N_{\text{ch}} \beta}{\dot{\beta}_{\max} T_s} \right] = 9.5 + \ln \left[ \left( \frac{N_{\text{ch}}}{10^9} \right) \left( \frac{\beta}{16 \text{ B}} \right) \left( \frac{10 \text{ GB/day}}{\dot{\beta}_{\max}} \right) \left( \frac{10 \text{ s}}{T_s} \right) \right], \quad (62)$$

where  $T_s$  is the integration time for one spectrum,  $\beta$  is the number of bytes recorded per threshold crossing or “hit,” and  $\dot{\beta}_{\max}$  is the maximum data recording rate. In Eq. 62 we have adopted parameters that typify near-future SETI spectrometers having  $\sim 10^9$  channels, such as BETA (HS93) and SERENDIP IV (Bowyer et al. 1994). The  $\sim 16$  bytes recorded per hit would give the sky position, time, frequency channel, signal amplitude, and some modest line-shape parameterization (e.g., whether it was unresolved, its width, etc.)

A semi-quantitative measure of the improvement offered by a lower threshold can be seen in Fig. 3. With a threshold of  $\eta_T = 10$ , the detection probability  $P_{2d}$  for an event at the survey threshold of META,  $\eta_1 = 32$ , is nearly a factor of  $10^2$  greater than with the threshold used. Similarly, dual-site observations employing thresholds of 10 rather than 16, e.g., META and META II, would have larger detection probabilities by a factor of  $\sim 10$ .

Whether a threshold as small as estimated is practical depends also on the extent to which spectral intensities depart from exponential statistics due to RFI, soft RAM errors, or celestial signals. From our considerations in previous sections, however, the hit threshold presented here would be more than adequate for a full statistical study of event amplitudes, especially if followed up with reobservations having a smaller number of channels (by a factor of  $10^3$ , say) and with a smaller threshold,  $\eta_T^{(\text{ro})} \sim 5$ . The data rate for reobservations would be substantially smaller than in the survey and would therefore not have an impact on the overall data rate. Follow-up analysis would include rejection of signals that appear in multiple sky positions and a search for signals that repeat in single sky positions (consistent with the telescope beam). Application of the Zepka et al. (1994) pdfCLEAN method would search for intensity histogram bins which have an excess of counts. In this regard,



pdfCLEAN can investigate signals at levels where noise produces a nonnegligible number of false-alarm threshold crossings.

The threshold in Eq. 62 is also adequate for two-station SETI, which can tolerate half the threshold of single-station SETI for roughly the same false-alarm rate.

For intensities below the hit threshold, we advocate computation of a histogram of S/N for a generous number of subbands of frequency channels and for a set of individual sky positions. This low-intensity histogram provides the means for identifying low-level RFI that persists in specific frequency bands and allows redundancy testing for signals that repeat in more than one sky position.

In summary, for future SETI we advocate a survey threshold given by  $\eta_T$  in Eq. 62 and where a modest amount of information is stored per hit (e.g., 16 bytes). Signals below the survey threshold would be recorded only as a count in a histogram calculated for a given subband of frequency channels and a coarse sky position.

### 13. SUMMARY AND CONCLUSIONS

In this paper we have discussed how interstellar scintillations cause intermittency in SETI and we have developed a formalism based on both the likelihood function and a Bayesian analysis for analyzing existing and future surveys. We emphasize that our results are based on the case where interstellar scintillations are saturated, producing modulations with a one-sided exponential distribution. This situation applies for distances beyond a frequency-dependent minimum distance, approximately a few hundred parsecs at 1 GHz. Our conclusions do not apply, quantitatively, for SETI that targets nearby stars using centimetric wavelengths, as in Project Phoenix (Tarter 1994). However, scintillation effects from the solar wind and from the stellar wind of the host star of transmitting sites will influence search sensitivities. These situations can also be analyzed using the methods of this paper.

In applying our methods to existing surveys we have found that:

- In META (Horowitz & Sagan 1993), considering each candidate separately, it is extremely unlikely that any of the 9 candidates with amplitude  $\geq 33\sigma$  was a mere noise fluctuation. A real signal, terrestrial or extraterrestrial, must underly these events. However, we are unable to distinguish between a steady signal modulated above threshold by scintillations and a transient signal, such as RFI, soft RAM errors, or transient ETI signals themselves.

- If any of the events in META is due to a scintillating celestial source, it likely results from a modest to large scintillation gain *combined* with a favorable noise fluctuation.
- We also show that existing reobservations of META candidate signals (i.e., those performed to date) are incapable of ruling out the case where a real ETI source with constant, intrinsic signal strength underlies the measured candidate signal. This conclusion holds even for the case where the scintillations remain correlated between the time of an initial detection and prompt reobservations. Future reobservations are certainly capable of ruling out a constant-source model for META detections.
- A stronger test of our signal models and of the celestial nature of candidate signals requires much lower thresholds and a larger number of reobservations than have been performed to date. For META, a reobservation threshold of 5–10 (in signal-to-noise ratio) rather than the actual 20 is needed. The number of reobservations needed is a function of threshold but is many thousands for the threshold used. In future surveys, correlated reobservations made promptly after the initial survey detection can drastically lower the total number of reobservations needed to rule out constant-strength ETI signal hypotheses.
- Dual-site observations made simultaneously are unlikely to yield dual detections of a source unless “low” thresholds are used for recording signal levels.

Having developed these formalisms and applied them to existing surveys, we also present recommendations for planning future surveys. An important recommendation concerns the philosophy regarding events below threshold. In Horowitz & Sagan (1993), nearly all events below threshold were discarded. As a result, in this paper, we have treated all such events equally, since the only information reported was that the intensity was below threshold. In doing so, we have nevertheless illustrated that, with the appropriate combination of scintillations and noise, observed intensities of, say,  $32\langle N \rangle$  can be explained by scintillating sources. If such scintillating sources do exist, then there must be many occasions in which the intensity would have been below threshold. We recommend the following strategies, based upon the methods described in Zepka, Cordes, & Wasserman (1994), for establishing the existence of and recovering these signals:

- A minimalist strategy would retain only those events exceeding a threshold (defined by the usual false-alarm probability), but would form a histogram of those events below threshold. Since the expected distribution of the noise is known, viz. a one-sided exponential, then *deviations* from this histogram indicate the presence of non-noise signals. Of course, separating RFI from actual ETI signals still remains a problem, requiring new observations.

- The optimal strategy would retain individual intensity values even for those that are far below the false-alarm threshold. Clustering on the sky of results from multiple scans of the sky would suggest the locations of extraterrestrial sources that could be subjected to intense scrutiny by the flotilla of existing astronomical instrumentation.

Application of our low-threshold strategy requires archiving of spectral amplitudes at large data rates. Our suggestion is that, given the large expense for conducting SETI, the data recorded and archived should be of commensurate cost and at a volume dictated by hardware available in the current market.

We thank P. Horowitz, T. Lored, J. Tarter, and D. Werthimer for helpful discussions. We also thank J. Tarter for organizing a workshop on intermittency in SETI, co-chaired by Carl Sagan, and co-sponsored by the Planetary Society, that was held at the SETI Institute in 1994 January. We thank the referee, B. Rickett, for comments that helped clarify the paper. Finally, JMC and TJWL thank Carl Sagan for decades of inspiration in general and for his enthusiasm and clarity on the subject matter of this article in particular. His last comment to us about the paper was that “...it may very well lead to the ultimate success of SETI.” This work was supported by the National Astronomy and Ionosphere Center, which operates the Arecibo Observatory under a cooperative agreement with the NSF, and by the Planetary Society,

## APPENDICES

### A. Symbols Used

Symbol	Definition
I,II,III	Denotes Model I, II, or III.
$\alpha$	The exponent in the log $N$ -log $S$ distribution of transmitters.
$B_D$	Spectral domain in which ETI signals are transmitted.
$\beta$	The number of bytes recorded per threshold crossing, or “hit.”
$\dot{\beta}_{\max}$	The maximum data recording rate in bytes $s^{-1}$ .
$\mathcal{C}$	The set of candidate signals found in a survey.
cro	Denotes reobservations with correlated scintillations.
$D_{\text{mfp}}$	Mean free path for the line of sight intersecting a source.
$\epsilon_{\text{ch}}$	Fraction of spectrometer channels containing ETI signals.
$\epsilon_{\text{RFI}}$	Fraction of all observations that include terrestrial RFI signals.
$\epsilon_{\text{sky}}$	Fraction of telescope beams containing ETI sources.
$\eta \equiv I/\langle N \rangle$	The intensity measured in units of the mean background noise.
$\eta_c \equiv I/\langle N \rangle$	The normalized intensity of a candidate.
$\eta_T \equiv I_T/\langle N \rangle$	The intensity threshold for detection.
$f(\eta \mathcal{I})$	The <i>posterior</i> pdf for the measured, normalized intensity given the background information $\mathcal{I}$ .
$f(\boldsymbol{\theta} \eta\mathcal{I})$	<i>Posterior</i> pdf for a set of parameters $\boldsymbol{\theta}$ given measurements of the normalized intensity $\eta$ and background information $\mathcal{I}$ .
$f_{\text{I,II,III}}$	The <i>posterior</i> pdf for Model I, II, or III.
ded $f_g(g)$	The pdf of the scintillation modulation (or gain), $g$ .
$f_{2g}(g_1, g_2; \rho)$	The bivariate pdf for two values of the scintillation gain $g_{1,2}$ as a function of the correlation coefficient $\rho$ .
$f_I(I, S)$	Intensity pdf for a constant source strength.

Symbol	Definition
$f_{I,\text{scint}}(I, S)$	Intensity pdf for a source that varies due to scintillations.
$f_{2I}(I_1, I_2; S, \rho)$	The bivariate intensity pdf.
$f_{\text{RFI}}(\zeta_{\text{RFI}})$	The pdf of normalized RFI source strengths.
$f_S(S)$	The pdf for the intrinsic source strength of ETI transmitters.
$f_{\boldsymbol{\theta}}(\boldsymbol{\theta})$	The <i>a priori</i> pdf for a set of parameters $\boldsymbol{\theta}$ .
$f_{\zeta}(\zeta)$	Pdf of normalized source strengths based on the spatial distribution and intrinsic radiated powers of ETI sources.
$g$	Scintillation “gain” for a compact source’s radio flux.
$g_c$	Scintillation gain applicable to a particular candidate event.
$H_G$	Half-thickness of the galactic disk.
$\mathcal{I}$	Background information in Bayesian analysis.
$I$	Intensity.
ISS	Interstellar scintillation or scattering.
$\delta I$	The rms variation in intensity.
$\Delta I$	The uncertainty in establishing intensities during a survey.
$I_0(x)$	The modified Bessel function of order 0.
$I_{\text{cand}}$	Intensity of a candidate from a search program.
$I_T$	Intensity threshold in a search program.
$K_r$	Number of reobservations of a candidate signal.
$K_{r,c}$	Number of reobservations where the ISS gain is <i>correlated</i> with the gain for the original candidate signal.
$K_{r,u}$	Number of reobservations where the ISS gain is <i>uncorrelated</i> with that for the original candidate detection.

Symbol	Definition
$[K_{r,c}]_{\text{crit}}$	Critical number of correlated reobservations needed to exclude the reality of survey candidate
$[K_{r,u}]_{\text{crit}}$	Critical number of uncorrelated reobservations needed to exclude the reality of a survey candidate.
$K_s$	Number of separate observations of each sky position in a survey.
$\mathcal{L}$	Likelihood function for a candidate signal.
$\mathcal{L}_{\text{cand}}$	Likelihood function for the candidates from a survey.
$\mathcal{L}_{\text{non}}$	Likelihood function for the non-detections in a survey.
$\lambda \equiv \log \mathcal{L}$	Log likelihood function for an individual candidate signal.
$\Lambda$	Total log likelihood function for an entire survey.
$\ell_d$	Characteristic length scale of the diffraction pattern.
$\ell_D$	Typical distance between transmitters.
$\ell_{\text{min,max}}$	Maximum and minimum distances of Galactic transmitters.
$\mathcal{N}$	The set of nondetections in a survey.
$N$	Noise intensity.
$\langle N \rangle$	Ensemble average noise intensity.
$N_b$	Number of Galactic transmitters in a telescope beam.
$N_{\text{cand}}$	Number of candidate signals found in a survey.
$N_{\text{ch}}$	Number of frequency channels in a SETI spectrometer.
$n_D$	Number <i>density</i> of transmitters.
$N_D$	Number of ETI transmitters in the Galaxy.
$\tilde{N}_D$	Number of sources such that $\ell_D = H_G$ .
$\Delta N_{\text{fa}}$	Number of false alarms expected per frequency channel.
$N_{\text{frames}}$	Number of reference frames assumed for Doppler shifts.

Symbol	Definition
$N_{\text{lines}}$	Number of distinct spectral lines transmitted by an ETI source.
$N_{\nu}$	Number of separate center frequencies searched.
$N_{\text{pol}}$	Number of polarizations searched.
$N_{\text{signals/beam}}$	Number of spectral lines from all ETI sources in a telescope beam.
$N_{\text{sky}}$	Number of sky positions (telescope beam areas) searched.
$N_{\text{su}} = N_{\text{sky}}N_{\text{ch}}K_{\text{s}}$	Total number of statistical trials in a survey.
$N_{\text{trials}}$	Total number of statistical trials in a survey.
$N_{\text{trials,noise}}$	Number of trials of the noise in a survey.
$N_{\text{trials,ISS}}$	Number of trials of independent scintillations in a survey.
$\Delta\nu_{\text{d}}$	Characteristic “diffraction” bandwidth for scintillations.
$\Delta\nu_{\text{sb}}$	Characteristic broadening width for a spectral line.
$\Delta\nu_{\text{spectrometer}}$	Total bandwidth of a SETI spectrometer.
$\Omega_{\text{b}}$	Solid angle of a radio telescope’s primary beam.
$\mathcal{P}$	Power radiated by a transmitter, assumed to be radiated isotropically [effective isotropic radiated power (EIRP)].
$P(I)$	Probability that the intensity exceeds a value $I$ .
$P_g(g)$	Probability that the scintillation gain exceeds a value $g$ .
$P_{\text{d}}(I_{\text{T}}, S)$	Detection probability that a source with strength $S$ produces an intensity that exceeds a threshold $I_{\text{T}}$ .
$P_{\text{d,scint}}(I_{\text{T}}, S)$	Detection probability when a source of strength $S$ scintillates.
$P_{2\text{d}}(I_{\text{T}} I_1; S, \rho)$	Detection probability in a second observation given an initial detection with amplitude $I_1$ , a source strength $S$ , and scintillation correlation $\rho$ .
$P_{\text{fa}}$	Probability of a false-alarm detection.
$P_{\nu}$	Probability that a band of frequencies contains ETI signals.
pdf	Probability density function

Symbol	Definition
$\mathcal{R}$	Set of intensity upper limits in reobservations made on survey candidates.
$r \equiv \mathcal{L}_{\text{II}}/\mathcal{L}_{\text{III}}$	Ratio of likelihood functions for Model II to Model III.
$r_\epsilon \equiv \epsilon_{\text{ro}}/\epsilon_{\text{su}}$	Ratio of the fraction of pointings containing ETI transmitters for reobservations and survey.
$R_{\text{G}}$	Radius of the galactic disk.
$\rho_g(\tau)$	Normalized, temporal correlation function for the scintillation gain $g$ as a function of time lag $\tau$ .
$\rho_I(\tau)$	Normalized correlation function for the intensity.
$\rho_N$	Normalized correlation function for radiometer noise.
$\rho_s(\tau)$	Normalized spatial correlation function for the scintillation gain $g$ .
ro	Subscript or superscript to denote reobservations of candidates.
$S$	Intensity of ETI signal without any modification by scintillations.
$S_{1,2}$	Minimum & maximum fluxes of a galactic population of standard candles.
$S_{\text{RFI}}$	Intensity of a terrestrial RFI signal.
$S_{1,\text{RFI}}$	Maximum intensity of a terrestrial RFI signal.
$S_{0,\text{RFI}}$	Minimum Intensity of a terrestrial RFI signal.
su	Subscript or superscript for a quantity relevant to a survey.
$\Delta t_{\text{d}}$	Characteristic diffraction time scale for scintillations (strong scattering regime).
$T_{\text{s}}$	Integration time for one spectrum.
$\theta_{\text{b}}$	One dimensional beam width (FWHM) of a radio telescope’s primary beam.
uro	Subscript or superscript to denote <i>scintillation-uncorrelated</i> reobservations
$V_{\text{b}}$	Volume in the Galactic disk within a telescope beam.
$V_{\perp}$	Perpendicular speed by which the observing geometry to a source changes.

Symbol	Definition
$\zeta \equiv S/\langle N \rangle$	Source signal strength in units of the mean background noise.
$\zeta_{1,2}$	Minimum and maximum normalized fluxes of a galactic population of standard candle transmitters.
$\zeta_{(0,1),\text{RFI}}$	Minimum and maximum normalized RFI flux.
$\zeta_{\text{RFI}}$	RFI signal strength in units of the mean background noise.



## B. Intensity Statistics

Let the measured intensity (in a single channel of a spectrometer, say) be

$$I = |s + n|^2 \quad (\text{B1})$$

where  $n$  is complex, gaussian noise and  $s$  is a signal phasor of *fixed* amplitude. The mean intensity is

$$\langle I \rangle = S + \langle N \rangle \quad (\text{B2})$$

where  $S \equiv |s|^2$ ,  $N \equiv |n|^2$ , and the variance is

$$\sigma_I^2 = \sigma_N^2 + 2S\langle N \rangle. \quad (\text{B3})$$

For unsmoothed noise from a Fourier transform spectrometer, which we assume for the entirety of this paper,  $\sigma_N = \langle N \rangle$ .

The probability density function (pdf) of  $I$  for an intrinsic signal intensity  $S$  is

$$f_I(I; S) = \langle N \rangle^{-1} I_0 \left( \frac{2\sqrt{IS}}{\langle N \rangle} \right) \exp \left[ -\frac{(I + S)}{\langle N \rangle} \right] U(I), \quad (\text{B4})$$

where  $I_0$  is the modified Bessel function and  $U(I)$  is the unit step function (Goodman 1984). With no signal ( $S = 0$ ), the pdf becomes a one-sided exponential function. The pdf of  $\sqrt{I}$  is the Rice distribution (e.g., Papoulis 1991).

The realistic case, where the signal strength varies due to scintillations, requires that  $S \rightarrow gS$  in Eq. B4 where  $g$  is the appropriate scintillation “gain.” Over short time spans (much less than a characteristic scintillation time),  $g = \text{constant}$  and the pdf of the intensity is of the form of Eq. B4. However, over long time spans,  $g$  varies according to its own pdf,  $f_g(g)$ , and the resultant intensity pdf is obtained by integrating over the pdf of  $g$ :

$$f_{I,\text{scint}}(I; S) = \int dg f_g(g) f_I(I; gS). \quad (\text{B5})$$

For saturated scintillations,

$$f_g(g) = \exp(-g)U(g), \quad (\text{B6})$$

yielding

$$f_{I,\text{scint}}(I; S) = \langle I \rangle^{-1} \exp \left( -\frac{I}{\langle I \rangle} \right) U(I), \quad (\text{B7})$$

where  $\langle I \rangle = S + \langle N \rangle$ , as before.

The utility of the two pdf’s in Eqs. B4 and B7 is as follows. In surveys where the dwell time per sky position is much less than the scintillation time scale, the apparent source

strength,  $gS$ , is fixed, and Eq. B4 is the appropriate form of the pdf to use in calculating detection probabilities, etc. *of that source at that time*. In large scale surveys of many independent sky positions, candidate detections of real signals will preferentially select large values of the product  $gS$  and, most likely, will be predisposed toward selecting abnormally large values of the scintillation gain  $g$ . However, in reobservations of candidate signals selected from an initial survey, it is likely that the reobservations will span, *in toto*, many characteristic scintillation times. The scintillation gain for any real source will vary over its allowed domain according to the exponential pdf (for strong scattering). In assessing the detectability of the source in these multiple reobservations, one must use the second form of the intensity pdf, i.e., Eq. B7.

Throughout this paper, we assume that the strong scattering regime obtains. For completeness, we note that there are two other scattering regimes (LC98): The weak scintillation regime is marked by a nearly symmetric scintillation gain pdf with a considerably smaller variance and a much longer scintillation time scale ( $\sim 1$  day) than the strong scattering case. In the transition regime the gain pdf has no simple analytical form but, when compared to an exponential distribution, has a much longer tail to large  $g$  while having a much longer scintillation time (of order the time scale in weak scintillation). At 1 GHz, the weak scintillation regime extends to approximately 100 pc and the transition regime extends to approximately 500 pc. In order that there be sources within these two regimes, the number of civilizations in the Galaxy must exceed  $10^5$  and  $10^3$  for the weak and transition regimes, respectively. These numbers follow by simply calculating the  $N_D$  needed to make the mean distance between civilizations equal to 100 or 500 pc.

### B.1. Signal Detection and False-alarm Probabilities

To calculate the probability that the intensity exceeds a specified threshold,  $I_T$ , i.e., a “detection,” we integrate the appropriate pdf,

$$P_d(I_T; S) = P(I > I_T) = \int_{I_T}^{\infty} dI f_I(I; S), \quad (\text{B8})$$

for the case of a non-scintillating signal of strength  $S$  or a single observation of a scintillating signal of observed strength  $S \rightarrow gS$ , and

$$P_{d,\text{scint}}(I_T; S) = P(I > I_T) = \int_{I_T}^{\infty} dI f_{I,\text{scint}}(I; S), \quad (\text{B9})$$

for the case of many observations of a scintillating source.

For a scintillating source, the detection probability can be calculated exactly and is

$$P_{\text{d,scint}}(I_{\text{T}}; S) = \exp\left(-\frac{I_{\text{T}}}{S + \langle N \rangle}\right). \quad (\text{B10})$$

For a source of *observed*, fixed strength  $gS$ , there exists no closed form expression for Eq. B8, however.

If there is no signal,  $S = 0$ , the “detection” probability becomes the “false-alarm” probability, a measure of how often the intensity will exceed the detection threshold solely from noise fluctuations. This false-alarm probability is

$$P_{\text{fa}}(I_{\text{T}}) = P_{\text{d}}(I_{\text{T}}; S = 0) = \exp\left(-\frac{I_{\text{T}}}{\langle N \rangle}\right). \quad (\text{B11})$$

By restricting a survey to a certain false-alarm probability, one can specify  $I_{\text{T}}$ ; for example, a false-alarm probability of  $10^{-12}$  corresponds to  $I_{\text{T}} = 27.6\langle N \rangle$ . Detection thresholds are set in most surveys so that the “false-alarm” rate yields a small number of spurious “detections” over the course of the survey.

## B.2. Second Order Intensity Statistics

The scintillation gain varies on a characteristic time scale,  $\Delta t_{\text{d}}$ , defined previously. Later, we will need to consider the joint statistics of the scintillation gain and the intensity at pairs of times. The bivariate pdf for the scintillation gain (Goodman 1984) is:

$$f_{2g}(g_1, g_2; \rho) = \frac{1}{1 - \rho} \exp\left[-\frac{g_1 + g_2}{1 - \rho}\right] I_0\left[\frac{2\sqrt{g_1 g_2 \rho}}{1 - \rho}\right], \quad (\text{B12})$$

where  $\rho = \rho(\tau)$  is the temporal correlation function for the gain  $g$ , normalized as  $\rho(0) = 1$ . This function is roughly gaussian in form and has a width that is equal to the characteristic scintillation time of the source. The scintillation time, as remarked in §2.2, is strongly frequency, direction, and distance dependent but can be modeled fairly well (cf. Fig. 1). For reobservations made promptly such that  $\tau \ll \Delta t_{\text{d}}$ ,  $\rho \rightarrow 1$  and  $f_{2g}$  tends to a one sided exponential function multiplied by  $\delta(g_1 - g_2)$ . For long times between observations such that scintillations are independent,  $\rho \rightarrow 0$  and  $f_{2g}$  becomes the product of the two individual pdf’s for  $g_1$  and  $g_2$ .

From the bivariate pdf for  $g$ , we write the bivariate pdf for the intensity as

$$f_{2I}(I_1, I_2; S, \rho) = \int \int dg_1 dg_2 f_{2g}(g_1, g_2; \rho) f_I(I_1; g_1 S) f_I(I_2; g_2 S). \quad (\text{B13})$$

As with the scintillation gain, the intensities measured at two times are more highly correlated for time separations small compared to the scintillation time; conversely, they are statistically independent if the separations exceed the scintillation time. The *degree* of correlation, even at short time separations, need not be large, however, because this also depends on the signal to noise ratio. We write the intensity correlation function as

$$\rho_I(\tau) = \frac{\langle \delta I(t) \delta I(t + \tau) \rangle}{\langle \delta I^2(t) \rangle} \quad (\text{B14})$$

where we define  $\delta I$  as the deviation from the mean noise level

$$\delta I(t) \equiv I(t) - \langle N \rangle = g(t)S + \delta N + 2\sqrt{g(t)S}\mathcal{R}(n). \quad (\text{B15})$$

Defining the noise correlation function as

$$\sigma_N^2 \rho_N(\tau) \equiv \langle \delta N(t) \delta N(t + \tau) \rangle \quad (\text{B16})$$

we obtain, for lags  $\tau \ll \Delta t_d$ ,

$$\rho_I(t) \approx \left[ \frac{g(t)g(t + \tau)S^2 + \langle N \rangle^2 \rho_N(\tau) [1 + 2Sg(t)/\langle N \rangle]}{[g(t)S + \langle N \rangle]^2} \right]. \quad (\text{B17})$$

Note that  $\rho_I(0) = \rho_N(0) = 1$ . At a lag  $\tau = 0^+$  such that the noise has decorrelated completely (i.e., at a lag comparable to the time needed to calculate a single FFT in a digital Fourier-transform spectrometer), the intensity correlation is

$$\rho_I(0^+) \approx \begin{cases} (gS/\langle N \rangle)^2 & gS \ll \langle N \rangle; \\ 1/4 & gS = \langle N \rangle; \\ 1 & gS \gg \langle N \rangle. \end{cases} \quad (\text{B18})$$

Thus, even though the scintillation gain may be completely correlated over an observation interval, the intensity need not be. Moreover, at rare times, the noise itself can produce a large spike that decorrelates on a short time scale.

We find that large intensity excursions receive contributions from both noise and scintillation fluctuations. Even if the scintillations are highly correlated at two times, the noise will not be, and the intensities need not be. This property has important consequences for our ability to confirm weak, candidate signals as being real ETI sources.

It is useful to define a *conditional* detection probability for a measurement at a time  $\Delta t$  after an initial detection:

$$P_{2d}(I_T|I_1; S, \rho[\Delta t]) = P\{I_2 > I_T|I_1; S, \rho[\Delta t]\} = \int_{I_T}^{\infty} dI_2 f_{2I}(I_1, I_2; S, \rho[\Delta t]). \quad (\text{B19})$$

### B.3. Intensities at Spatially Separated Sites

Here we consider joint intensity statistics at two spatial locations for the purpose of analyzing SETI programs that involve simultaneous, dual station observations. Well separated sites provide a powerful means for rejecting RFI or instrumental effects that are peculiar to an individual site (Welch 1983). However, scintillations and system noise are also different, in general, at separated sites.

The intensities measured at two sites at locations  $\vec{x}_{1,2}$  will both be of the form of Eq. B1 with statistics as described in Eq. B2-B7. We must ask how the different elements of the intensity are correlated between the two locations.

The noise is uncorrelated, except for that resulting from any compact sources in the beams of the two telescopes that would be detected if the two antennas were used as an interferometer. At centimetric frequencies and for typical system temperatures, any correlated flux typically amounts to a very small fraction of the total system noise. Henceforth, we ignore any such correlated noise.

The scintillation gain  $g$  is generally not 100% correlated between two sites. In terms of the normalized, temporal correlation described in §B.2, the spatial correlation is  $\rho_s(\ell = V_\perp \tau) = \rho(\ell/V_\perp)$ , and where the characteristic width of  $\rho_s$  ranges between tens of km for a strongly scattered source and  $> 10^4$  km for a weakly scattered source observed at a frequency  $\nu = 1$  GHz. The spatial correlation length increases with frequency as  $\ell_d \propto \nu^{1.2}$ .

For an intrinsic source strength,  $S$ , the *modulated* source strength at the  $i^{\text{th}}$  site at time  $t_\alpha$  and frequency  $\nu_\beta$  is

$$S_{\alpha\beta i} = g(\vec{x}_i, t_\alpha, \nu_\beta) S(t_\alpha, \nu_\beta). \quad (\text{B20})$$

Between two sites, the signal is partially correlated, according to the value of  $\rho_s(\ell)$ . The noise at the  $i^{\text{th}}$  site is

$$N_{\alpha\beta i} = N(\vec{x}_i, t_\alpha, \nu_\beta) \quad (\text{B21})$$

and is uncorrelated between two different sites ( $\alpha \neq \alpha', \beta \neq \beta', i \neq j$ )

$$\langle N_{\alpha\beta i} N_{\alpha'\beta' j} \rangle = \langle N(\vec{x}_i, t_\alpha, \nu_\beta) \rangle \langle N(\vec{x}_j, t_\alpha, \nu_\beta) \rangle. \quad (\text{B22})$$

Generally, the cross-correlation of the signal portion of the intensity involves a multidimensional lag involving spatial separation, time lag, and frequency separation. We are interested in narrowband signals measured at identical times and we will consider the signals to be intrinsically constant (in time) and deterministic. For this case, if the only variation in signal between two sites is the spatial difference of the scintillation gain, then:

$$\langle (gS)_{\alpha\beta i} (gS)_{\alpha\beta j} \rangle = \langle g(\vec{x}_i, t_\alpha, \nu_\beta) g(\vec{x}_j, t_\alpha, \nu_\beta) \rangle S^2(\nu_\beta) = [1 + \rho_s(|\vec{x}_i - \vec{x}_j|)] S^2(\nu_\beta). \quad (\text{B23})$$

In practice, there is a Doppler shift of the signal between the two sites that must be accounted for and which provides useful means for assessing the celestial nature of a source. But as long as the Doppler shift is less than the characteristic bandwidth of the scintillations, Eq. B23 still applies. Larger Doppler shifts can be described by a similar equation, but with an effective  $\rho_s$  that is a combination of spatial and frequency correlations.

## REFERENCES

- Bowyer, S. Werthimer, D. & Donnelly, C. 1994, in Proceedings of the Santa Cruz Bioastronomy Conference, ed. S. Shostak (San Francisco: Astronomical Society of the Pacific), p. 285.
- Cohen, N. & Charlton, D. 1995, in *Progress in the Search for Extraterrestrial Life*, ASP Conference Series, Vol. 74, ed. G. S. Shostak, ASP: San Francisco, 313.
- Condon, J. J. 1974, ApJ, 188, 279
- Colomb, R., Hurrell, E., Olalde, J., & Lemarchand, G. 1993, in Third Decennial US-USSR Conference on SETI, ed. G. S. Shostak (San Francisco: Astronomical Society of the Pacific) p. 279
- Cordes, J. M. 1986, ApJ, 311, 183
- Cordes, J. M. & Lazio, T. J. 1993, in Third Decennial US-USSR Conference on SETI, ed. G. S. Shostak (San Francisco: Astronomical Society of the Pacific) p. 143 (CL93)
- Cordes, J. M., Romani, R. W. & Lundgren, S. C. 1993, Nature, 362, 133
- Cordes, J. M. & Lazio, T. J. 1991, ApJ, 376, 123 (CL91)
- Cordes, J. M. & Sullivan, W.T. III. 1995, in *Progress in the Search for Extraterrestrial Life*, ASP Conference Series, Vol. 74, ed. G. S. Shostak, ASP: San Francisco, .
- Dixon, R. S. 1985, in *The Search for Extraterrestrial Life: Recent Developments*, ed. M. D. Papagiannis (Dordrecht: Reidel) p. 305
- Drake, F. D. & Helou, G. 1977, “The Optimum Frequencies for Interstellar Communications as Influenced by Minimum Bandwidth,” NAIC report 76, unpublished
- Goodman, J. W. 1984, in *Laser Speckle and Related Phenomena*, ed. J. C. Dainty (Berlin:Springer-Verlag) p. 9

- Gray, R.H. 1994, *Icarus*, 112, 485
- Gregory, P. C. & Lored, T. J. 1992, *ApJ*, 398, 146
- Harrison, P.A. & Lyne, A. G. 1993, *MNRAS*, 265, 778
- Horowitz, P. & Sagan, C. 1993, *ApJ*, 415, 218 (HS93)
- Lazio, T. J. & Cordes, J. M. 1998, *ApJS*, submitted (LC98)
- Levin, S., Olsen, E.T., Backus, C. & Gulkis, S. 1995, in *Progress in the Search for Extraterrestrial Life*, ASP Conference Series, Vol. 74, ed. G. S. Shostak, ASP: San Francisco, 471.
- Lovelace, R.V.E. 1970, Ph.D thesis, Cornell University
- Lyne, A.G. & Lorimer, D. R. 1994, *Nature*, 369, 127.
- Oliver, B. M. 1973, Project Cyclops: A Design Study of a System for Detecting Extraterrestrial Life, Report CR 114445 (Moffett Field, CA: NASA/Ames Research Center)
- Papoulis, A. 1991, *Probability, Random Variables and Stochastic Processes*, Third Edition (New York: McGraw-Hill)
- Rickett, B. J. 1990, *ARA&A*, 28, 561
- Shklovskii, I.S. & Sagan, C. 1966, *Intelligent Life in the Universe*, (San Francisco:Holden-Day)
- Scheuer, P. A. G. 1974, *MNRAS*, 166, 329
- Tarter, J. C. 1994, *BAAS*, 184, 5401
- Taylor, J. H. & Cordes, J. M. 1993, *ApJ*, 411, 674
- Wasserman, I. 1992, *ApJ*, 394, 565
- Welch, W. J. 1983, in SETI Science Working Group Report, Eds. F. Drake, J.H. Wolfe & C.L. Seeger (NASA Technical Paper 2244), pp. 95–98.
- Zepka, A. F., Cordes, J. M. & Wasserman, I. 1994, *ApJ*, 427, 438

Fig. 1.— *Top*: Contours of the scintillation time scale as viewed looking down on the plane of the Galaxy. The + indicates the Galactic center and the dashed circles have radii of 5 and 10 kpc. The offset figure shows the assumed locations of the spiral arms. The scintillation times refer to an observation frequency of 1.42 GHz and for directions at zero Galactic latitude. The scintillation time scales with frequency as  $\nu^{1.2}$ . *Bottom*: Contours of the scintillation bandwidth at 1.42 GHz. The bandwidth scales with frequency as  $\nu^{4.4}$ .

Fig. 2.— Detection probabilities vs normalized source strength  $S/I_T$  for the case where the source does not scintillate (dashed line) and for the case where it does scintillate in the strong scattering regime (solid line).

Fig. 3.— Detection probability for a second detection above a threshold  $\eta_T = I_T/\langle N \rangle$  given an initial detection with intensity  $\eta_1 = I_1/\langle N \rangle$ . Curves are plotted as a function of  $\rho_g$ , which may be either the spatial or temporal correlation function of the scintillation gain. Curves are labelled with the *intrinsic* source strength  $\zeta = S/\langle N \rangle$ , i.e., the source strength in the absence of scintillations. *a*)  $\eta_1 = 32$ ,  $\eta_T = 20$ , typical META parameters; *b*)  $\eta_1 = 32$ ,  $\eta_T = 10$ , recommended reobservation threshold for future META-like surveys; *c*)  $\eta_1 = 16$ ,  $\eta_T = 16$ , typical dual-site META-META II parameters; *d*)  $\eta_1 = 10$ ,  $\eta_T = 10$ , recommended thresholds for future dual-site observations.

Fig. 4.— Representative time series for the three models for META events; the dashed lines indicate a detection threshold: *a*) Noise only. *b*) A scintillating source with amplitude  $gS = 5\langle N \rangle$  combined with noise. It is assumed that the scintillation gain is constant over the time series. *c*) A scintillating source with time-varying scintillation gain,  $g(t)$ , combined with noise. *d*) RFI pulse combined with noise.

Fig. 5.— The joint *a posteriori* pdf for the scintillation gain  $g_c$  and intrinsic signal strength  $\zeta = S/\langle N \rangle$ . Contours are at 95%, 90%, 50%, 10%, 1%, and 0.1% of the peak. The number of reobservations is assumed to be 256. *a*) For a candidate with  $\eta_c = 32$  and a reobservation threshold of  $\eta_T^{(\text{ro})} = 20$ , typical of the META survey. *b*) For  $\eta_c = 100$  and  $\eta_T^{(\text{ro})} = 20$ . *c*) For  $\eta_c = 32$  and  $\eta_T^{(\text{ro})} = 10$ . *d*) For  $\eta_c = 100$  and  $\eta_T^{(\text{ro})} = 10$ .

Fig. 6.— Best fit values for  $g_c$ ,  $\zeta$ , and their product  $g_c\zeta$  for an initial candidate detection plotted against the number of reobservations. It is assumed that the scintillation gain  $g$  is uncorrelated between reobservations and between any reobservation and the original survey detection. Results are shown for a survey amplitude  $\eta_c = 32$  and for three values of the reobservation threshold,  $\eta_T^{(\text{ro})} = 5, 15, \text{ and } 20$ . *a*)  $\zeta$  vs.  $K_{r,u}$ . *b*)  $g_c$  vs.  $K_{r,u}$ . *c*)  $g_c\zeta$  vs.  $K_{r,u}$ .



Fig. 7.— [Top] The critical number of reobservations  $[K_{r,u}]_{\text{crit}}$  plotted against reobservation threshold  $\eta_{\text{T}}^{(\text{ro})}$ .  $[K_{r,u}]_{\text{crit}}$  is the number of reobservations needed for a given reobservation threshold  $\eta_{\text{T}}^{(\text{ro})}$  in order to render Model II highly improbable. The curves are labelled by the intensity of the candidate signal,  $\eta_c$ , at the initial detection. [Bottom] The number of false alarm detections expected (per frequency channel) in  $[K_{r,u}]_{\text{crit}}$  reobservations. The dashed line designates one false alarm per frequency channel, an unacceptably large number.

Fig. 8.— Similar to Fig. 6, but where correlated reobservations,  $K_{r,c}$ , are included in the analysis. *a)* Candidate intensity  $\eta_c = 32$  and reobservation threshold  $\eta_{\text{T}}^{(\text{ro})} = 20$ . *b)*  $\eta_c = 32$  and  $\eta_{\text{T}}^{(\text{ro})} = 10$ . *c)*  $\eta_c = 32$  and  $\eta_{\text{T}}^{(\text{ro})} = 5$ .

Fig. 9.— As for Fig. 7 but for *correlated* reobservations  $[K_{r,c}]_{\text{crit}}$ .

Fig. 10.— Contours of the logarithm of the survey likelihood functions for the META candidates. Contours are at 95%, 90%, 50%, 10%, 1%, and 0.1% of the peak in each panel. *a)* The survey likelihood function, including reobservations, of the four META candidates at 1420 MHz assuming Model II, namely a population of standard candle transmitters in the Galactic disk which are modulated by scintillation. *b)* As for (*a*), but for the seven 2840 MHz candidates. *c)* As for (*a*), but for Model III, namely RFI. *d)* As for (*b*), but for Model III, namely RFI.

Fig. 11.— The fraction of the sky having ETI sources in the telescope beam,  $\epsilon_{\text{sky}}$ , as a function of the mean free path for a beam to intersect an ETI source. We assume a uniform galactic disk of radius 15 kpc and thickness 0.2 kpc.

Fig. 12.— The number of sources  $N_{\text{D}}$  plotted against survey fraction  $\epsilon_{\text{su}}$ . The solid curve is the estimate for  $N_{\text{D}}$  obtained from Eq. 55 while the dashed line results from Eq. 57.

Table 1. SETI PROGRAM PARAMETERS

Parameter	META	META II	SERENDIP III
$N_\nu$	2	1	5
$N_{\text{frames}}$	3	3	1
$N_{\text{ch}}$	$2^{23}$	$2^{23}$	$2^{22}$
$N_{\text{pol}}$	2	2	1
$N_{\text{sky}}$	$10^{5.2}$	$10^{5.0}$	$10^{5.8}$
$K_s$	4	1	2.3 (ave)
$N_{\text{trials}}$	$10^{13.8}$	$10^{13.2}$	$10^{13.9}$
Beam size (deg)	0.5 (1.42 GHz) 0.25 (2.84 GHz)	0.5 (1.42 GHz)	0.15 (0.42 GHz)
$\Delta\nu_{\text{ch}}$ (Hz)	0.05	0.05	0.6
$\Delta\nu_{\text{total}}$ (MHz)	0.4	0.4	12
dwell time (s)	20	20	1.7
Thresholds:			
survey	$31.7\langle N \rangle$	$24\langle N \rangle$	$15\langle N \rangle$
reobserve	$20\langle N \rangle$	...	...
Sensitivities: (EIRP = effective isotropic radiation power.)			
EIRP ( $\text{W m}^{-2}$ )	$10^{-22.8}$		$10^{-24.6}$

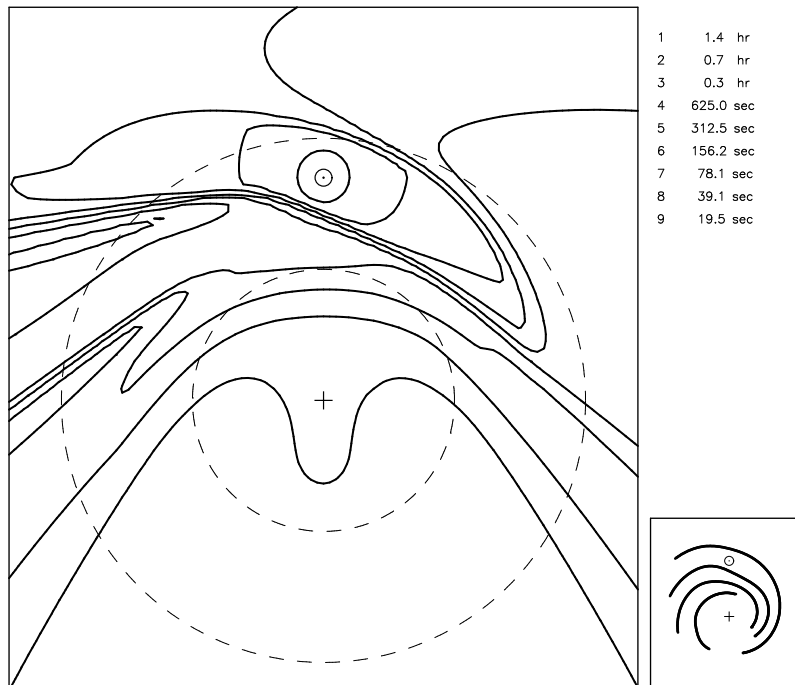
Table 2. Bayesian Maxima for META

$\eta_c$	$\eta_T$	$g_c$	$\zeta$
32	20	6.2	2.6
100	20	16.3	3.9
32	10	$< 10^{-3}$	$< 10^{-1}$
100	10	22.0	2.0

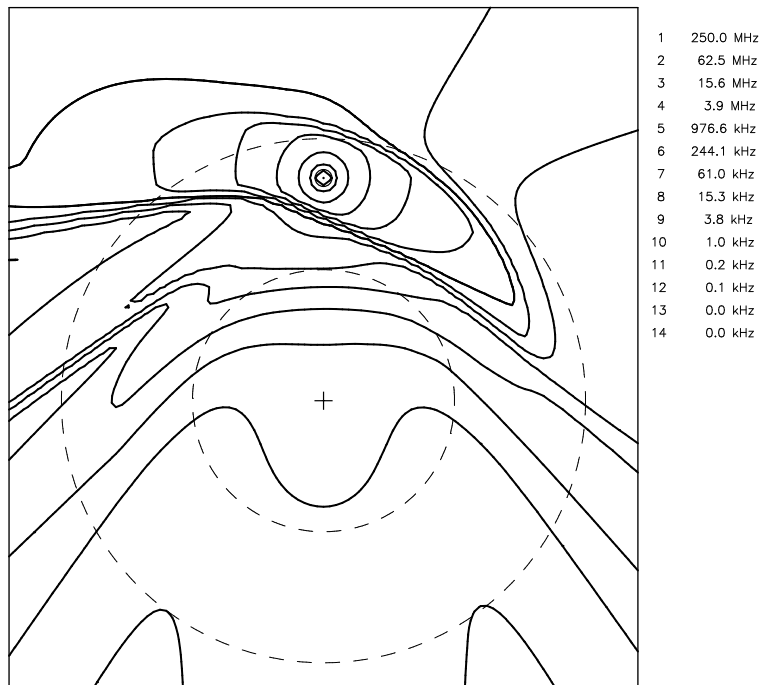
Table 3. Likelihood Maxima for META

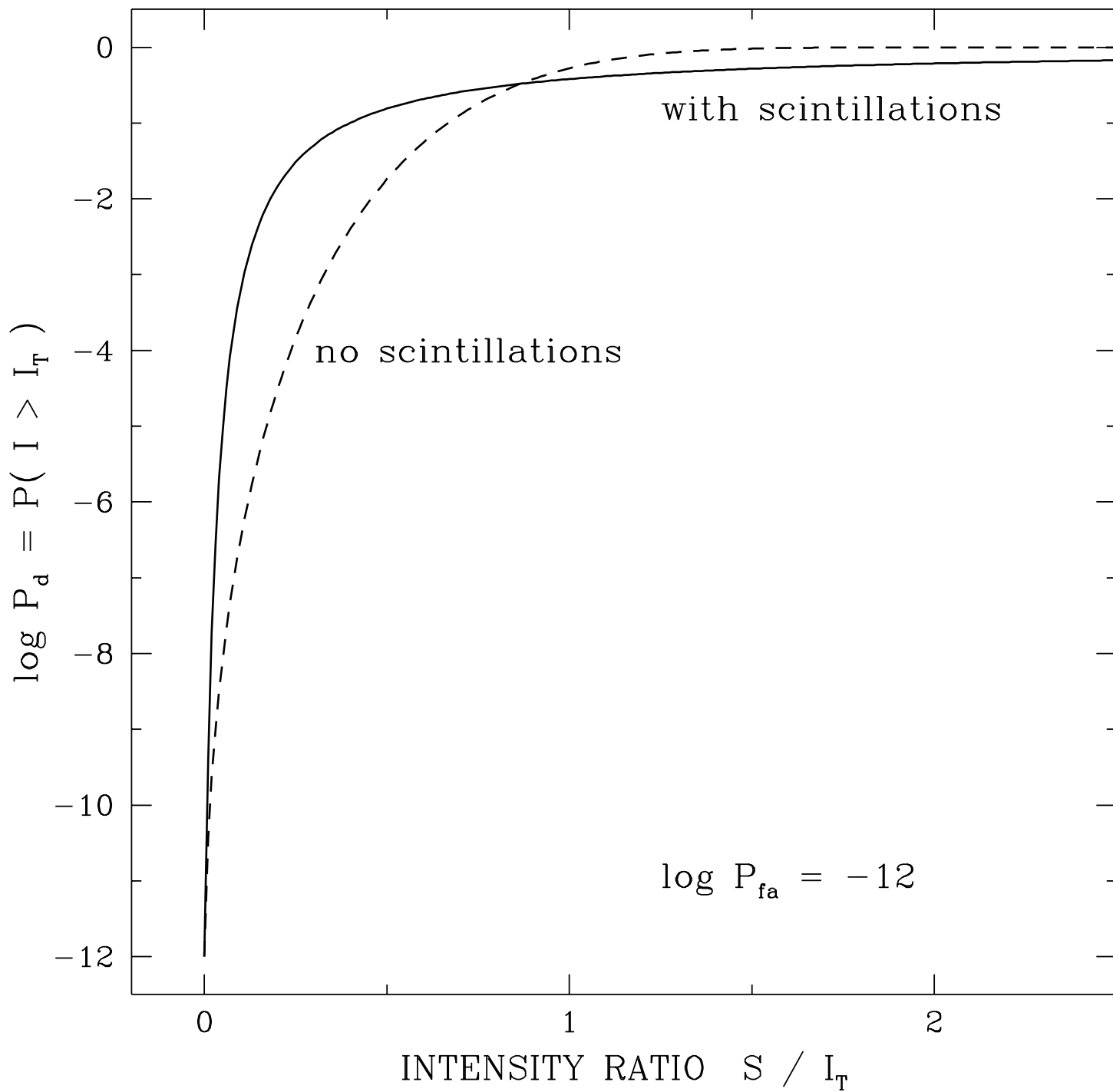
$\nu$ (MHz)	$\max(\Lambda)$	$\zeta_0 \epsilon_{\text{su}}$	$\zeta_1$
Model II: Survey			
1420	-61.6	$10^{-11.9}$	$10^{2.78}$
2840	-107	$10^{-11.6}$	$10^{3.54}$
Model II: Survey+Reobservations			
1420	-61.6	$10^{-11.9}$	$10^{2.78}$
2840	-107	$10^{-11.6}$	$10^{3.54}$
Model III: Survey			
1420	-61.3	$10^{-13.6}$	$10^{2.42}$
2840	-108	$10^{-13.2}$	$10^{2.91}$
Model III: Survey+Reobservations			
1420	-61.3	$10^{-13.6}$	$10^{2.42}$
2840	-108	$10^{-13.2}$	$10^{2.91}$

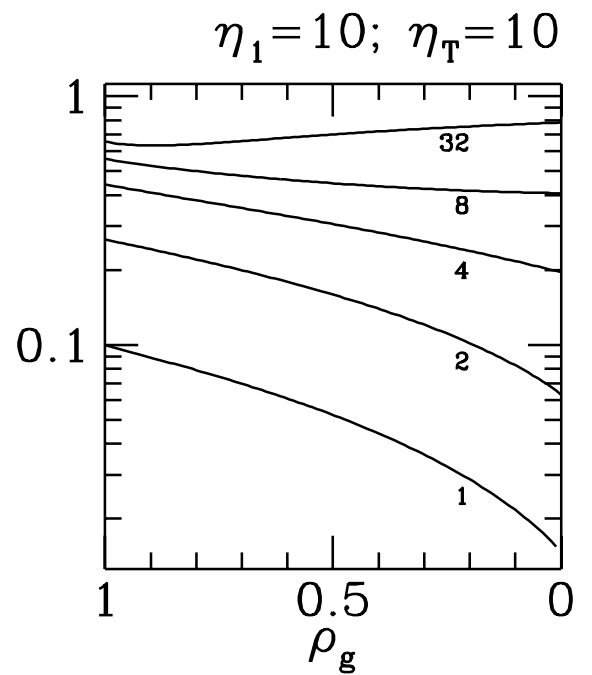
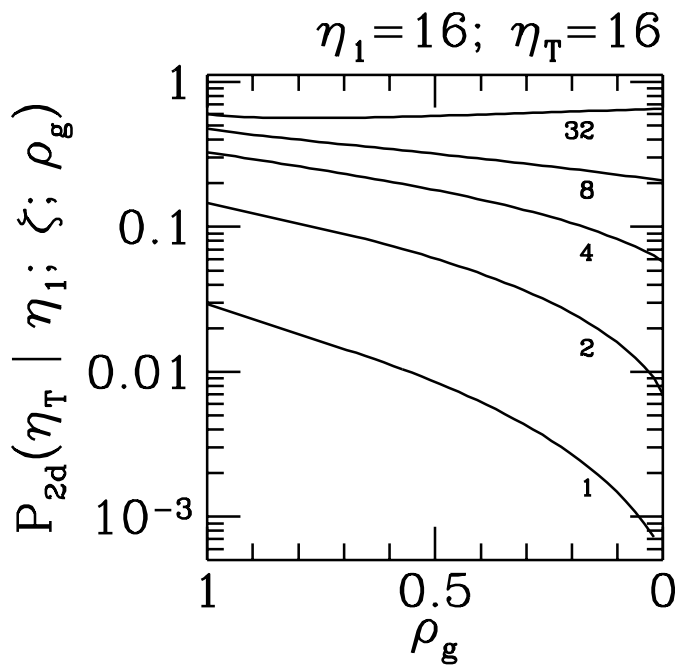
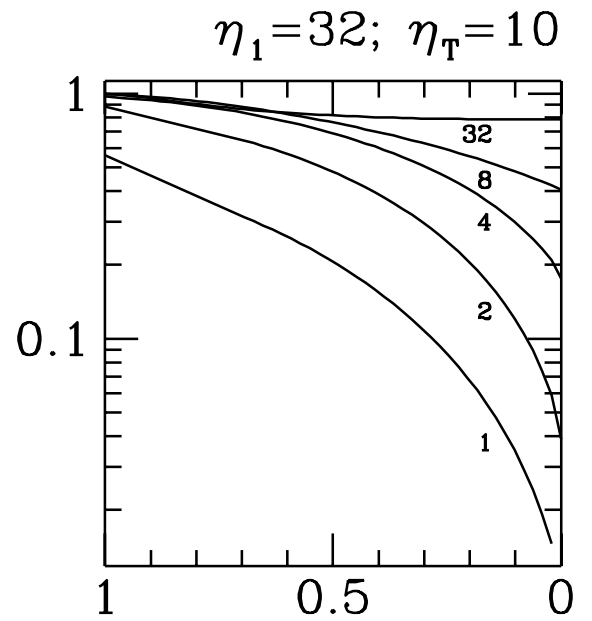
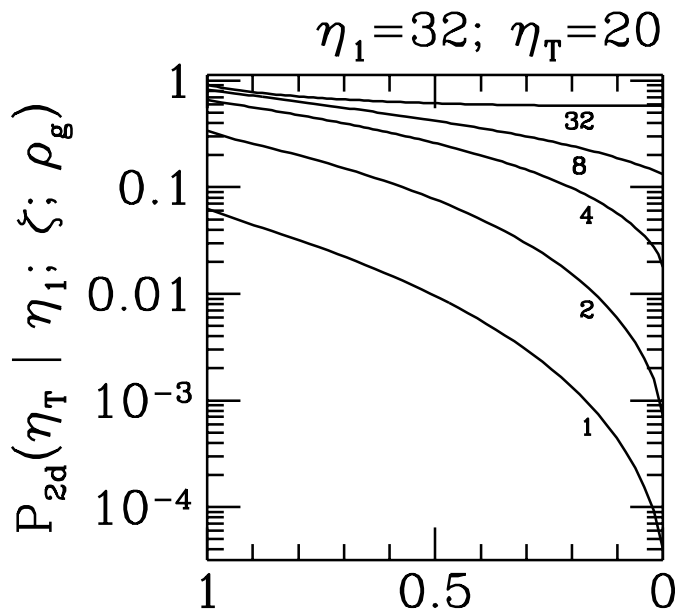
### CONTOURS OF SCINTILLATION TIME

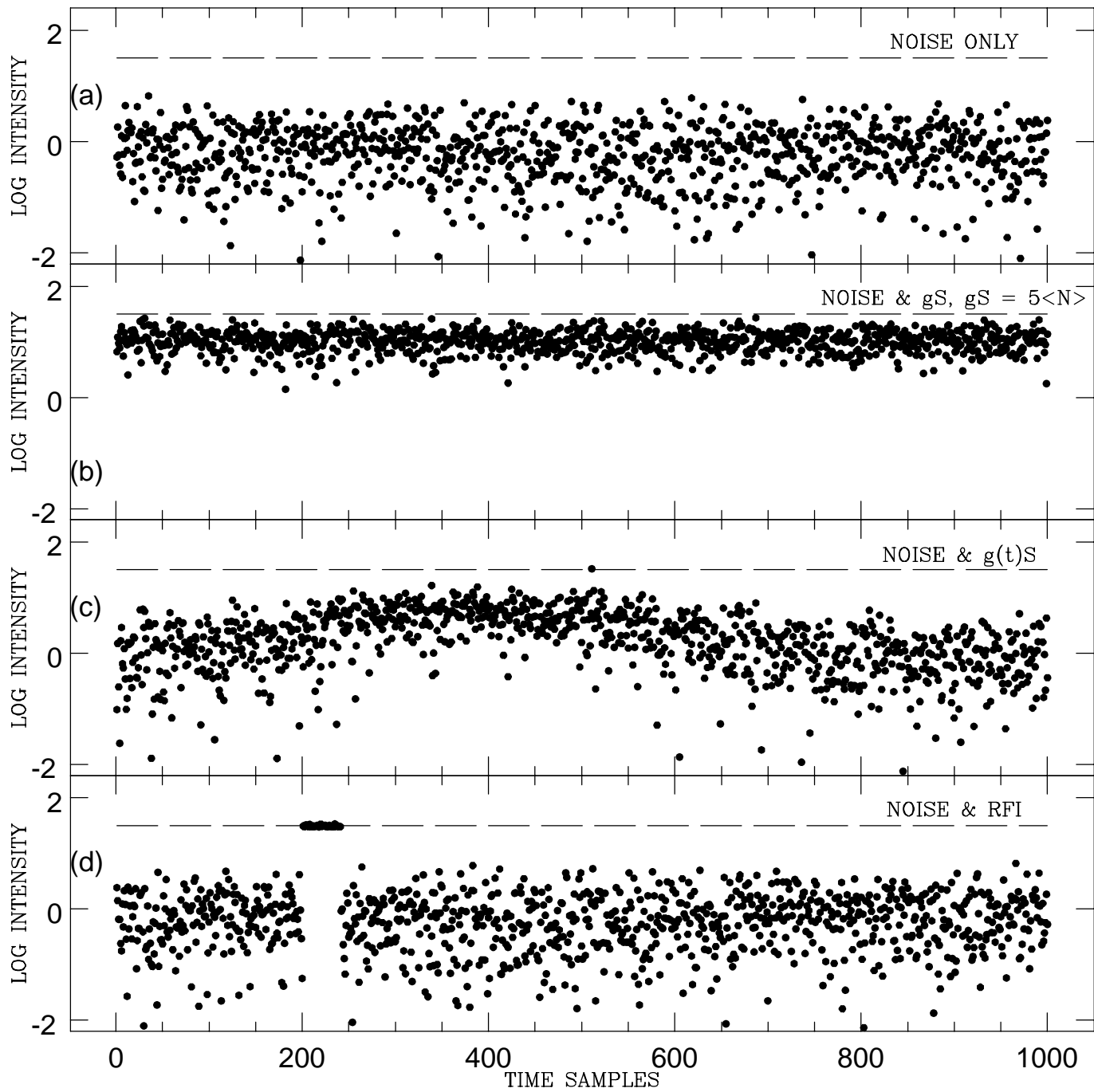


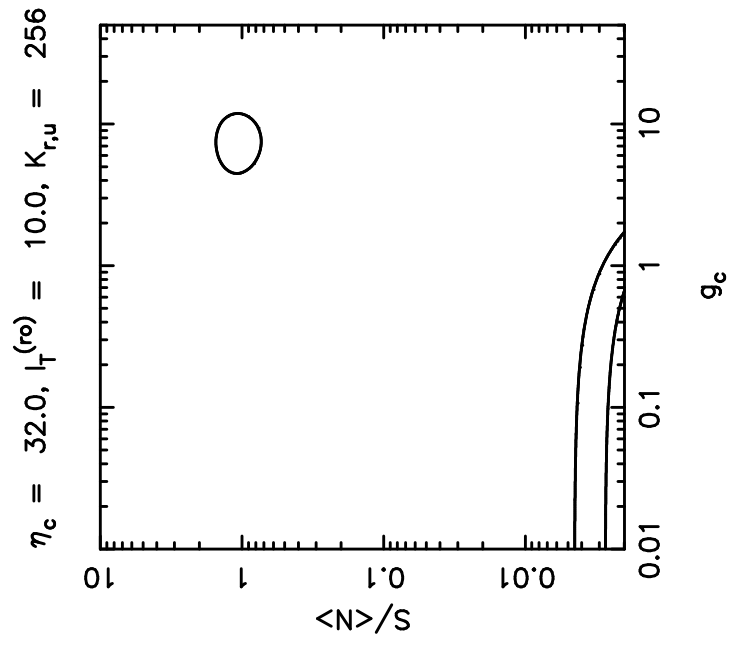
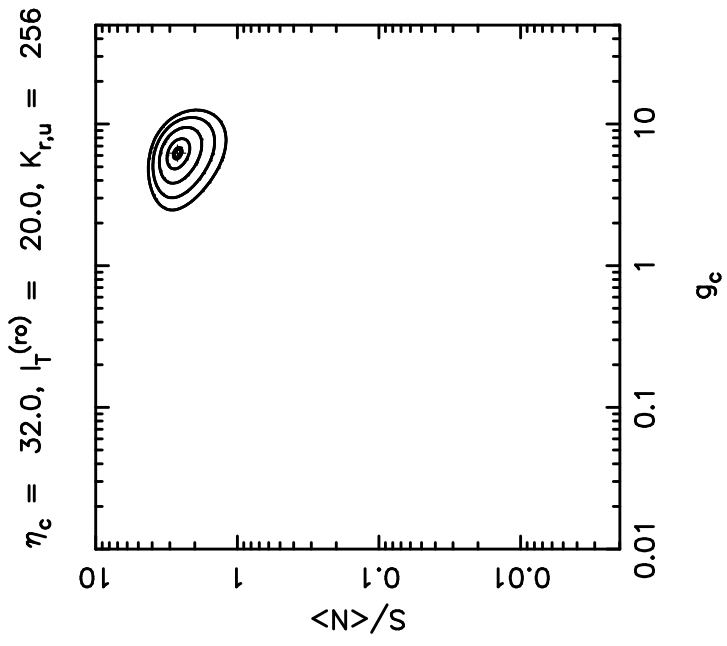
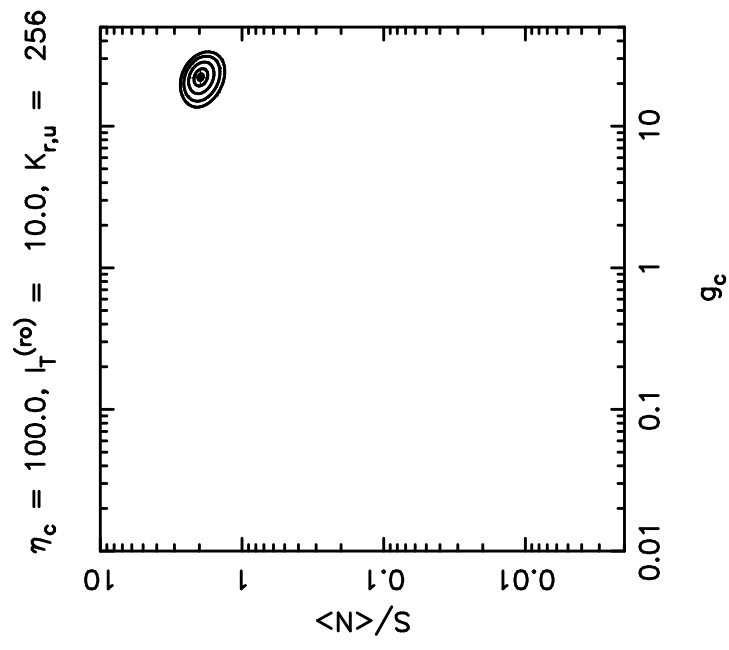
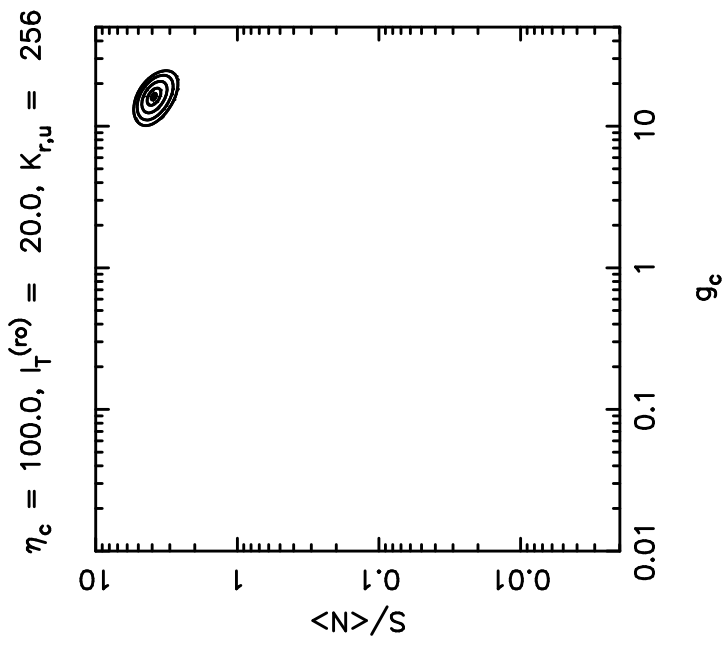
### CONTOURS OF SCINTILLATION BANDWIDTH



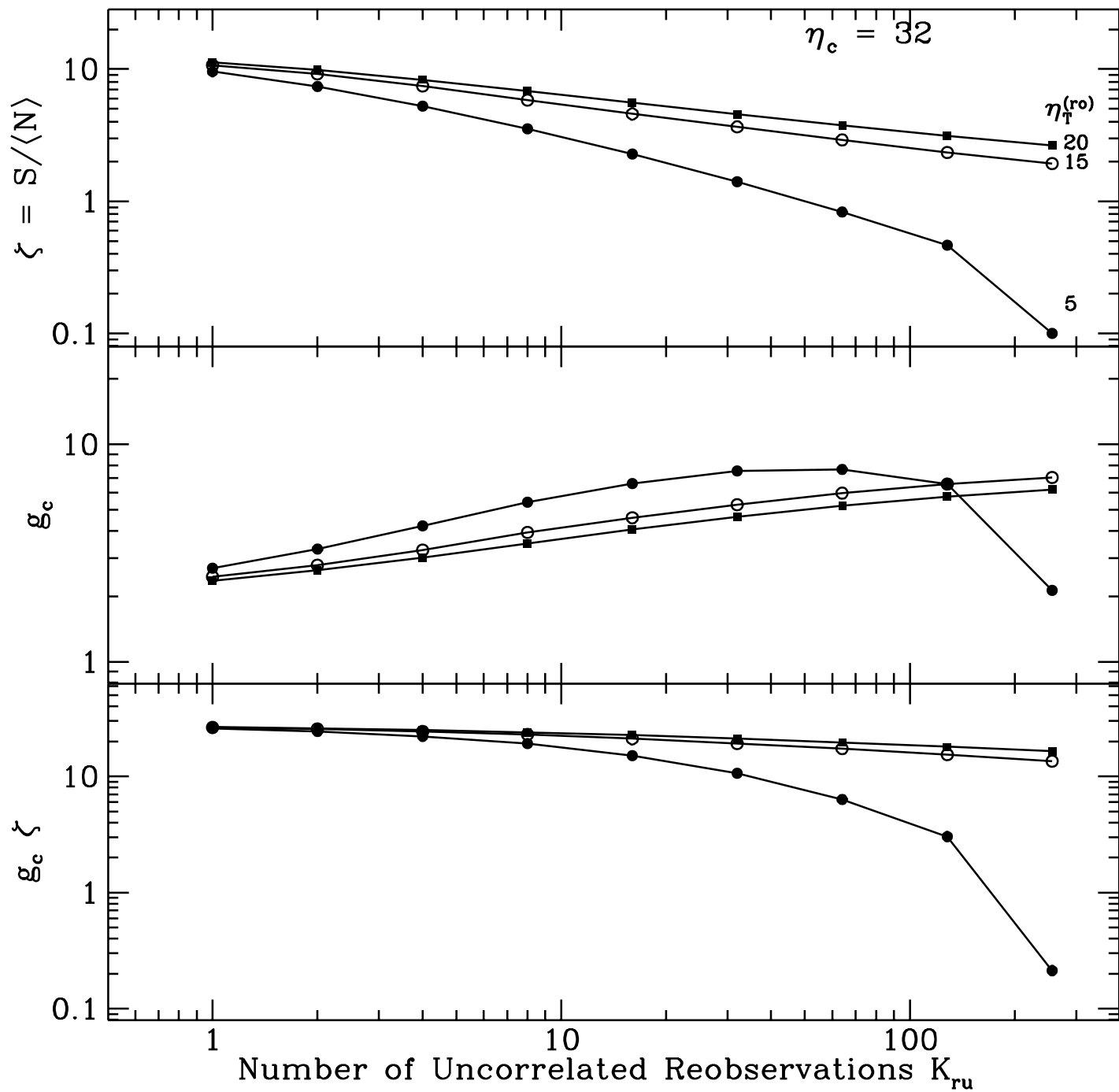


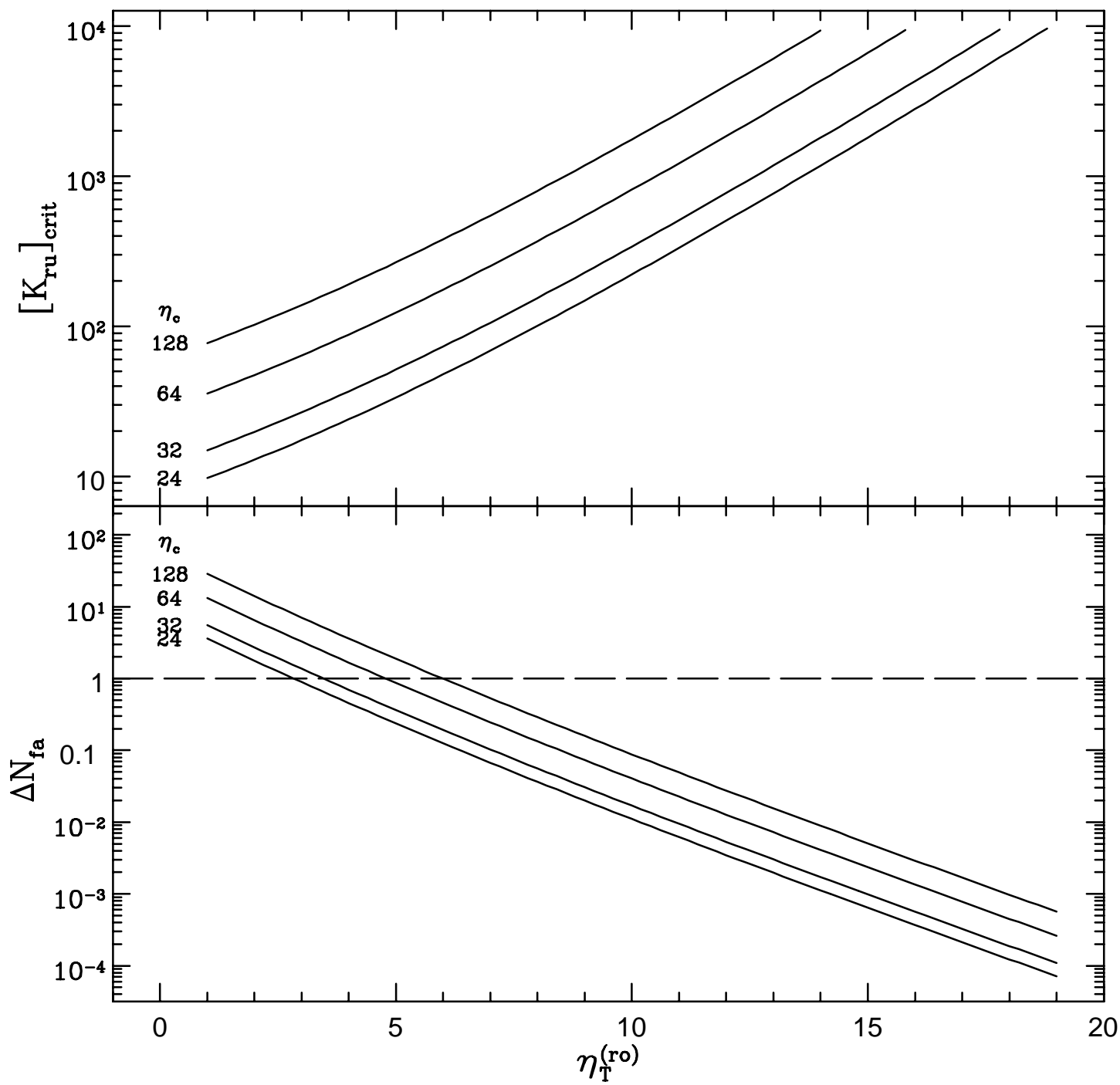


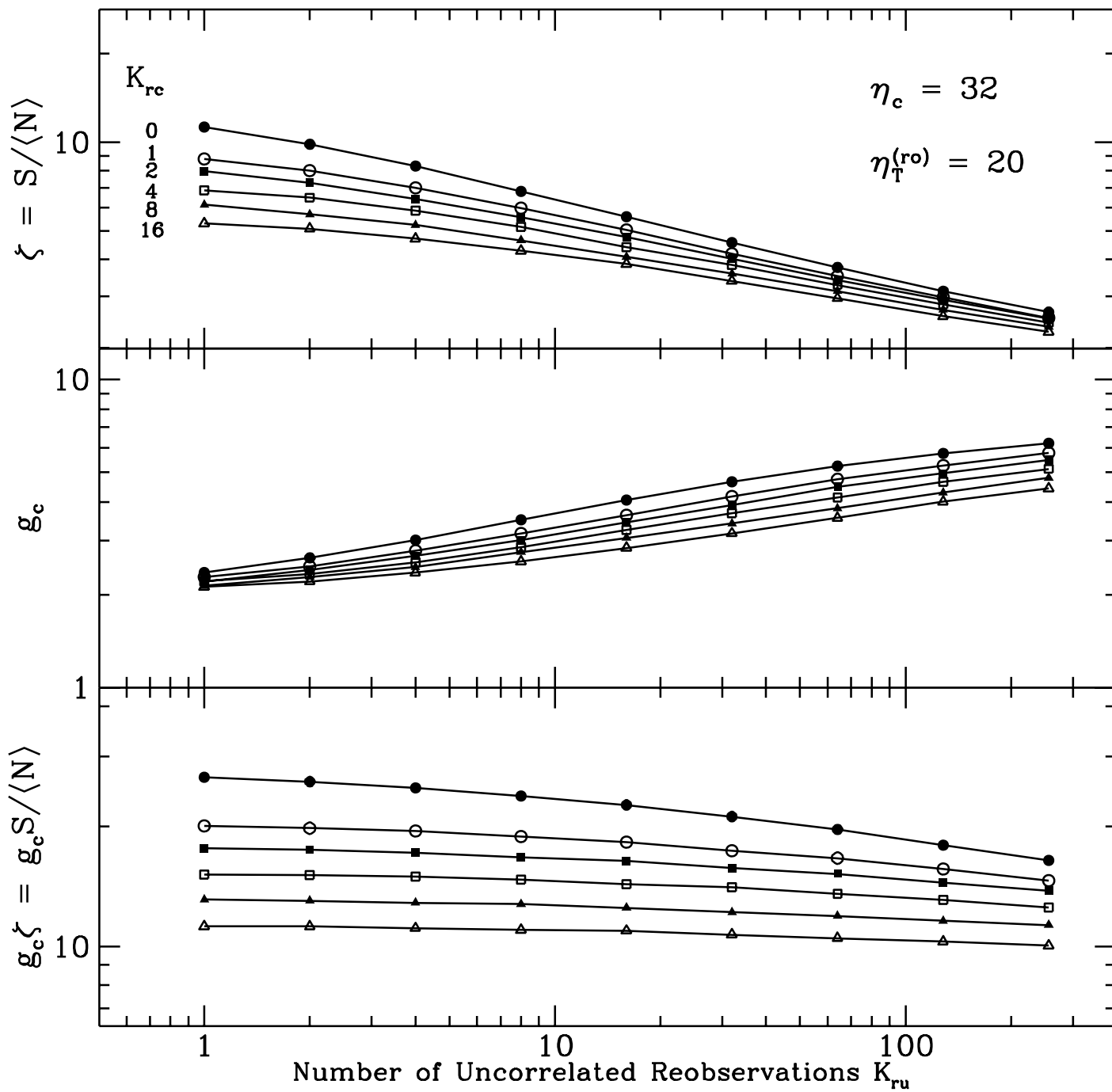


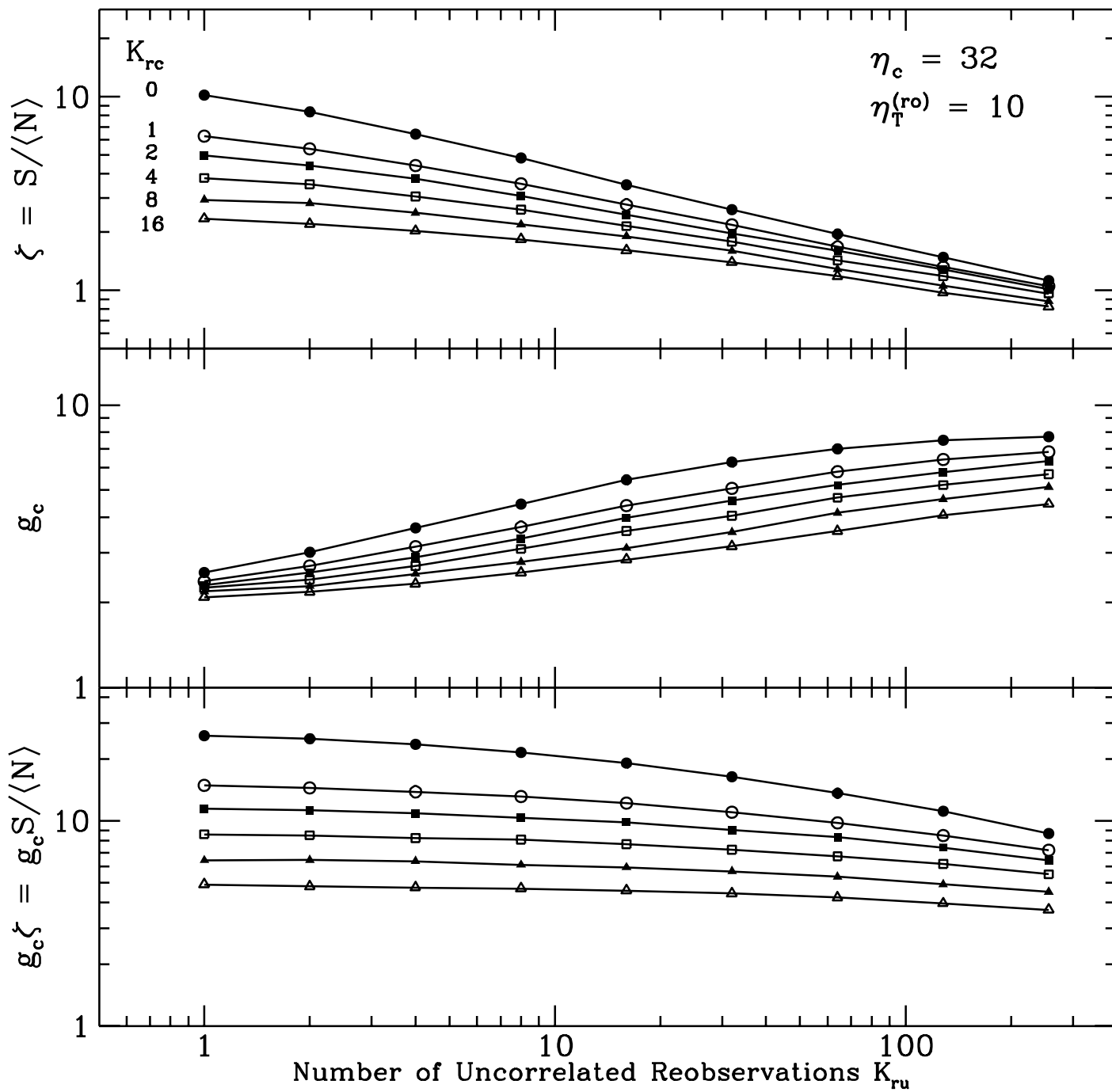


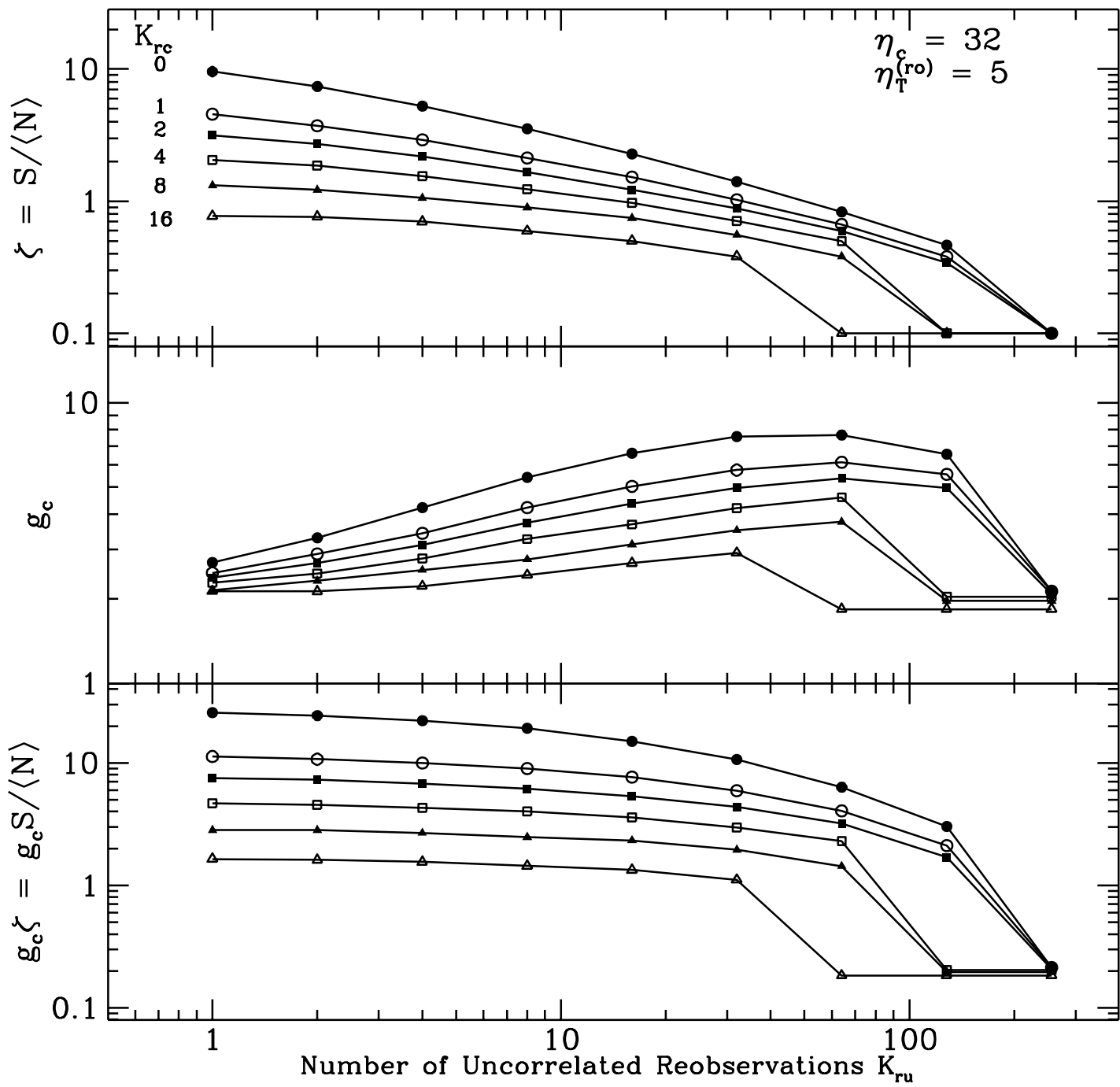


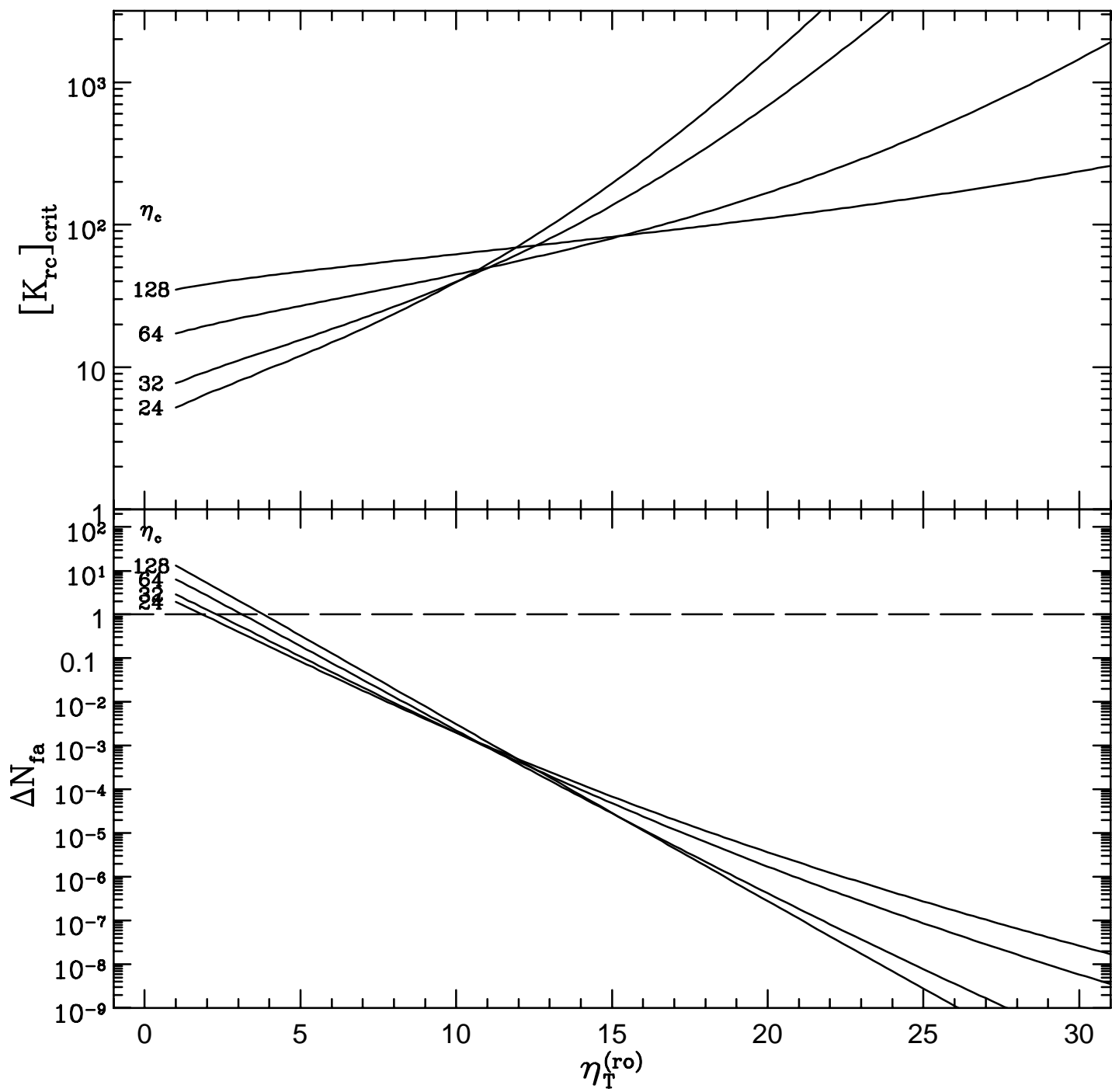






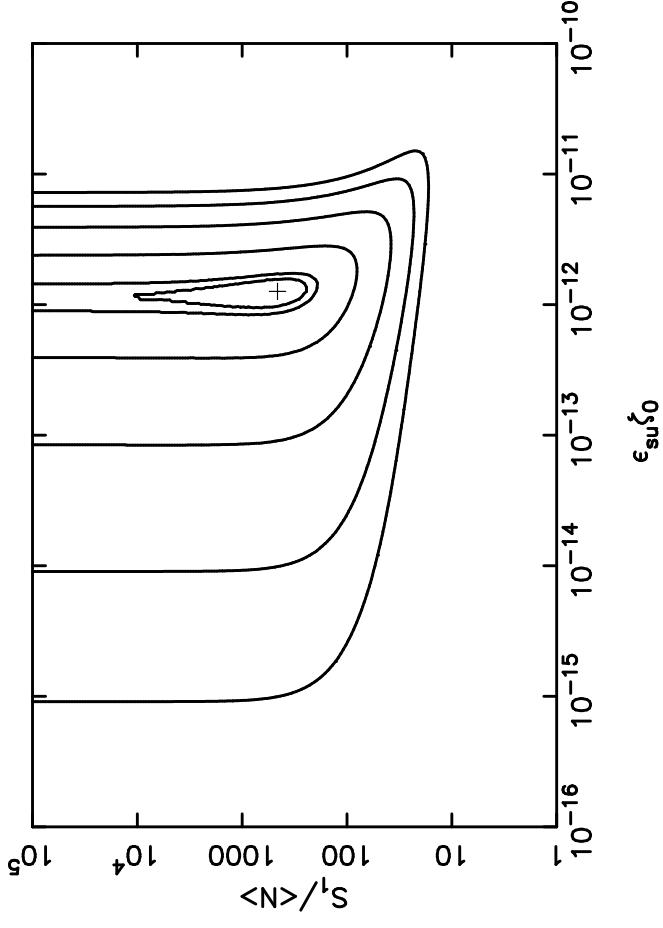






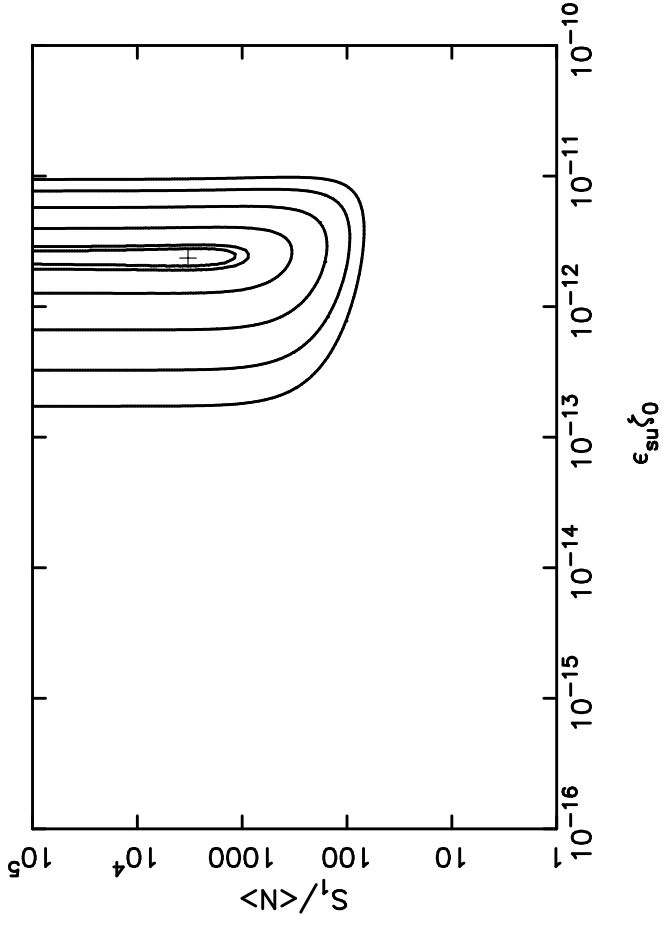
1420 MHz

Survey+Reobservations



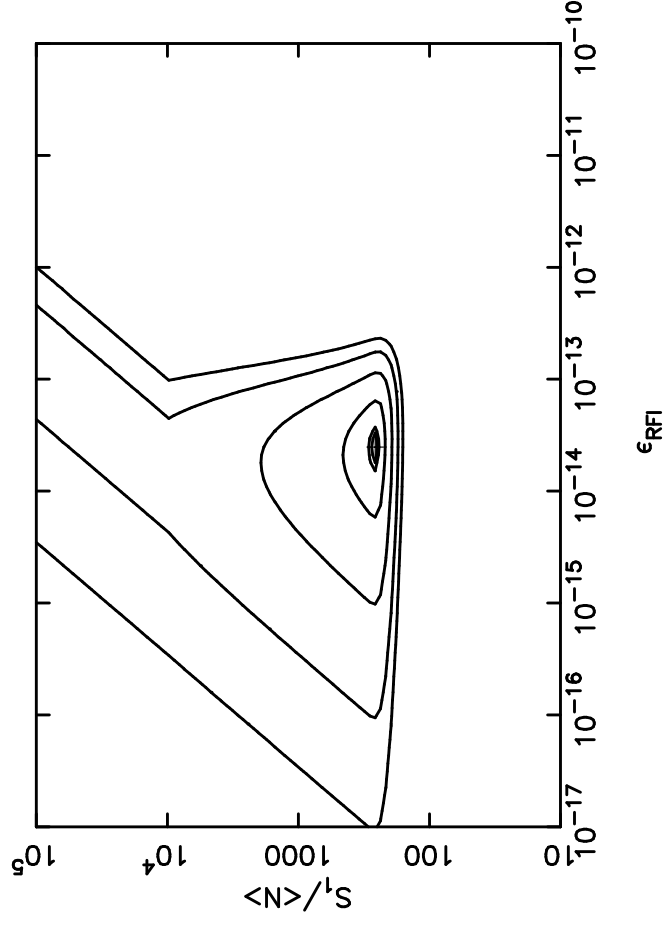
2840 MHz

Survey+Reobservations



1420 MHz

Survey+Reobservations



2840 MHz

Survey+Reobservations

